AD-A019 322

THE GALVANIC CORROSION OF GRAPHITE EPOXY COMPOSITE MATERIALS COUPLED WITH ALLOYS

Bennie A. Miller. Jr.

Air Force Institute of Technology
Wright-Patterson Air Force Base, Ohio

December 1975

DISTRIBUTED BY:

NTIS
National Technical Information Service
U. S. DEPARTMENT OF COMMERCE

THE GALVANIC CORROSION OF GRAPHITE EPOXY COMPOSITE MATERIALS COUPLED WITH ALLOYS

THESIS

GAE/MC/75D-8

Bennie A. Miller Jr.
Captain USAF

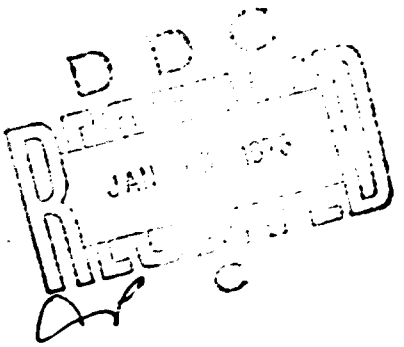

A

UNCLASSIFIED

SECURITY CLASSIFICATION OF THIS PAGE (When Data Entered)

REPORT DOCUMENTATION PAGE		READ INSTRUCTIONS BEFORE COMPLETING FORM
1. REPORT NUMBER GAE/MC/75D-8	2. GOVT ACCESSION NO.	3. RECIPIENT'S CATALOG NUMBER
4. TITLE (and Subtitle) THE GALVANIC CORROSION OF GRAPHITE EPOXY COMPOSITE MATERIALS COUPLED WITH ALLOYS		5. TYPE OF REPORT & PERIOD COVERED AFIT THESIS 6. PERFORMING ORG. REPORT NUMBER
7. AUTHOR(s) Bennie A. Miller Jr., Capt, USAF		8. CONTRACT OR GRANT NUMBER(s)
9. PERFORMING ORGANIZATION NAME AND ADDRESS Air Force Institute of Technology (AFIT/EN) WPAFB, OH 45433		10. PROGRAM ELEMENT, PROJECT, TASK AREA & WORK UNIT NUMBERS
11. CONTROLLING OFFICE NAME AND ADDRESS		12. REPORT DATE 13. NUMBER OF PAGES 49
14. MONITORING AGENCY NAME & ADDRESS(if different from Controlling Office)		15. SECURITY CLASS (of this report) UNCLASSIFIED 15a. DECLASSIFICATION/DOWNGRADING SCHEDULE

16. DISTRIBUTION STATEMENT (of this Report)

Approved for public release; distribution unlimited.

17. DISTRIBUTION STATEMENT (of the abstract entered in Block 20, if different from Report)

18. SUPPLEMENTARY NOTES

Approved for public release; IAW AFR 190-17

Jerry C. Hix, Captain, USAF
Director of Information

19. KEY WORDS (Continue on reverse side if necessary and identify by block number)

Galvanic Corrosion
Graphite Epoxy
Composite Material

20. ABSTRACT (Continue on reverse side if necessary and identify by block number)

A controlled laboratory study was made of the galvanic corrosion that occurs when graphite-epoxy composite material (GECM) is coupled with various alloys in neutral 3.5% aqueous NaCl at room temperature. These tests simulated GECM/alloy joints that occur in aerospace applications. Previous work has shown that GECM acts as an extremely noble metal when coupled with a limited number of alloy types such as aluminum and titanium. This study extends this research by considering more alloy types; namely, steels, stainless steels, nickel base, copper, as well as aluminum and titanium. Four types of GECM were used along

DD FORM 1 JAN 73 1473 EDITION OF 1 NOV 65 IS OBSOLETE S/N 0102-014-6601 UNCLASSIFIED

SECURITY CLASSIFICATION OF THIS PAGE (When Data Entered)

with pure graphite. Twenty-three alloys were tested for compatibility with GECM. Electrochemical test methods included potential measurements and galvanic current measurements. Galvanic current was measured by the use of a potentiostat modified to operate as a zero-resistance ammeter. Weight-loss tests were also conducted.

Conclusions derived from the results of this study are: (1) galvanic series based upon potentials are a poor indicator of GECM/alloy galvanic corrosion, (2) monitoring of galvanic current indicates the time dependent variations of galvanic corrosion better than weight-loss tests, (3) aluminum alloys and steels are least compatible with GECM, stainless steels and Be-Cu are more compatible, and nickel base and titanium alloys show excellent compatibility, (4) acceptability by particular alloy is as follows: Acceptable-Ti-6Al-4V, Ti-6Al-2Sn-4Zr-2Mo, Rene 41, Inconel X, Inconel, AFC-77, PH 17-7, SS-304, Be-Cu, SS-301, Borderline-Aluminum Graphite, MA-87, SS-440C, Al-2024-TG, Al-2024 T3, 1020, Al-7075-T6, 4130, Unacceptable-10 Ni Mod, 300M, Al-2020-T651, and 4340, (5) magnitudes of corrosion potentials of GEC materials were similar and close to that of pure graphite, and (6) no particular GECM was found superior, or inferior, in reducing galvanic corrosion.

THE GALVANIC CORROSION OF GRAPHITE EPOXY COMPOSITE MATERIALS COUPLED WITH ALLOYS

THESIS

Presented to the Faculty of the School of Engineering

of the Air Force Institute of Technology

Air University

in Partial Fulfillment of the

Requirements for the Degree of

Master of Science

by

Bennie A. Miller Jr., B.S.A.E.
Captain USAF

Graduate Aerospace-Mechanical Engineering

December 1975

Approved for public release; distribution unlimited.

Preface

I selected a corrosion related research investigation because of an originally casual interest in the ever-recurring, expensive, and time-consuming corrosion problems involved in maintaining a fleet of aging B-52 bombers. Corrosion was a constantly cited reason for equipment failure, especially on electronic equipment. It was the cause of flight cancellations, delays, and training loss. I hope that my work on this research effort helps me contribute something toward controlling corrosion on USAF weapon systems. It is hoped that the data accumulated, the analysis made, and the conclusions drawn from this study can be of immediate use and provide a basis for future research.

The lengthy section on electrochemical corrosion theory presented in this paper may seem overly detailed for a report primarily concerned with presenting experimental data. I feel, however, that the discussion of this theory greatly aids in the understanding of the method of using galvanic current measurement in predicting galvanic corrosion rates. This method is relatively new, and certainly not widely disseminated. Also, information on the subject is scattered and comes from many sources. It is hoped that my attempt to bring together pertinent galvanic corrosion information and to relate this information to basic electrochemical corrosion theory aids in the understanding of both the method and the results of this investigation.

This investigation has been both a rewarding experience, and, at times, a frustrating ordeal. Many hours of laboratory experimentation, library research, and study have made this paper possible. Without the guidance and encouragement of both Lieutenant Colonel James A. Snide,

my thesis advisor, and Mr. Sylvester G. Lee, this investigation would not have been possible. Mr. Lee also provided invaluable technical assistance in the laboratory, provided an abundance of literature relevant to the research, and gave expert advice when questions arose. I am indebted to Lieutenant Peter F. Dexter of AFFDL-FEM for assistance in acquiring test materials and equipment; Mr. Paul L. Burley of Hercules, Incorporated, for providing graphite epoxy composite test material; the AFIT School Shop personnel for their technical suggestions and fabrication of test specimens. A last special thanks goes to my wife who provided clerical assistance and who, most of all, was always there with kind words and understanding when problems seemed overwhelming.

Bennie A. Miller Jr.

Contents

List of Figures

List of Tables

Abstract

A controlled laboratory study was made of the galvanic corrosion that occurs when graphite-epoxy composite material (GECM) is coupled with various alloys in neutral 3.5% aqueous NaCl at room temperature. These tests simulated GECM/alloy joints that occur in aerospace applications. Previous work has shown that GECM acts as an extremely noble metal when coupled with a limited number of alloy types such as aluminum and titanium. This study extends this research by considering more alloy types; namely, steels, stainless steels, nickel base, copper, as well as aluminum and titanium. Four types of GECM were used along with pure graphite. Twenty-three alloys were tested for compatibility with GECM. Electrochemical test methods included potential measurements and galvanic current measurements. Galvanic current was measured by the use of a potentiostat modified to operate as a zero-resistance ammeter. Weight-loss tests were also conducted.

Conclusions derived from the results of this study are: (1) galvanic series based upon potentials are a poor indicator of GECM/alloy galvanic corrosion, (2) monitoring of galvanic current indicates the time dependent variations of galvanic corrosion better than weight-loss tests, (3) aluminum alloys and steels are least compatible with GECM, stainless steels and Be-Cu are more compatible, and nickel base and titanium alloys show excellent compatibility, (4) acceptability by particular alloy is as follows: Acceptable-Ti-6Al-4V, Ti-6Al-2Sn-4Zr-2Mo, Rene 41, Inconel X, Inconel, AFC-77, PH 17-7, SS-304, Be-Cu, SS-301, Borderline-Aluminum-Graphite, MA-87, SS-440C, Al-2024-T6, Al-2024-T3, 1020, Al-7075-T6, 4130,

Unacceptable-10 Ni Mod, 300M, Al-2020-T651, and 4340, (5) magnitudes of corrosion potentials of GEC materials were similar and close to that of pure graphite, and (6) no particular GECM was found superior or inferior in reducing galvanic corrosion.

THE GALVANIC CORROSION OF GRAPHITE EPOXY COMPOSITE MATERIAL COUPLED WITH ALLOYS

I. Introduction

Purpose

The purpose of this investigation was to study the galvanic corrosion that occurs when an alloy is coupled with Graphite Epoxy Composite Material (GECM) and immersed in an electrolyte. An anticipated application of the results of this study would be the provision of a guideline to be used in the selection of fastener or bearing alloys to be coupled with GECM. Four types of GECM were used as a basis for tests to determine if the corrosion properties of GECM are general in nature. Pure graphite samples were also tested to show that GECM corrosion properties are similar to those of pure graphite.

Alloys investigated included several that are commonly used on aircraft and space structures and a few that are proposed for aerospace application. Specifically, alloys from the following major alloy types were evaluated: (1) aluminum alloys, (2) steels, (3) stainless steels, (4) titanium alloys, (5) nickel-based alloys, and (6) beryllium copper.

The electrolyte, or corrosive medium, used for galvanic testing was a 3.5% sodium chloride (NaCl) solution at ambient temperature. This electrolyte composition was chosen for three reasons. First, it simulates the NaCl content of natural seawater. Second, it has been found that iron and steel alloys have their highest corrosion rate in this NaCl concentration (Ref 1:98). Finally, a large number of investigators have used this electrolyte as a basis for their work which makes data comparison a much easier task.

Immersion of the alloy/GECM couple in 3.5% NaCl and the use of electrochemical experimental apparatus produced data which was tabulated according to the couples corrosion resistance. These data also indicated the variation of galvanic corrosion parameters with time.

The method selected for collecting galvanic corrosion data was the use of a potentiostat modified to operate as a zero resistance ammeter (ZRA). This electrochemical method was chosen because it allows measurement of very small currents with least error. The method also reduced test duration by making possible the evaluation of several couples in a relatively short time.

Background

Graphite epoxy composite material is one of the relatively new materials known as advanced composites. Its existence is due to the technological progress made in the non-metallic materials field during the last decade. It is composed of high strength-high modulus graphite fibers combined with an amine cured polymer epoxy resin (Ref 2:1.1). The graphite fiber is produced by burning polyacrylonitrile (PAN) in air and then carbonizing it in an inert atmosphere at a much higher temperature. This process produces continuous filament bundles of graphite fiber which can be woven, twisted, or chopped and then impregnated with selected epoxy resins to form various shapes such as sheets, tubes, and even extruded structural members.

Its primary advantage for aerospace application is its high strength to weight ratio (Ref 2:1.1). Typical weight savings of 25% to 50% have been demonstrated on aircraft components. For example, on the A-37B aircraft main landing gear side brace, the GECM replacement part withstood ultimate loads and endured the required four fatigue lifetimes with

a weight reduction of 35% over the aluminum alloy part (Ref 3:6). Table I lists several applications of GECM on operational aerospace components, and some proposed applications.

Because of its high strength to weight ratio, GECM is being considered for many aerospace components. There is, however, a potentially disadvantageous property. Graphite behaves electrochemically like a noble metal such as gold or platinum. This nobility results in an electrical potential difference which causes galvanic current to flow when GECM is coupled to a less noble metal or alloy in an electrolyte. The less noble metal or alloy corrodes due to galvanic action. Galvanic corrosion of aluminum alloys has occurred on aircraft parts when the corrosive medium is tapwater (Ref 4:33) or seawater (Ref 5:8), and has been found to be severe. Because of the galvanic corrosion problem, an important consideration in component design where GECM is a proposed material would be the corrosion compatibility of alloy/GECM joints. The prime motivation for conducting this experimental research is to determine the extent to which galvanic effects increase the corrosion rates of various alloys that might be fastened to GECM.

COMPONENT	COMPANY
F-5 leading edge wing tip. (First GECM structure to be flown in U.S.)	Northrop
Integral rib-stiffened panels	Northrop
F-5 leading edge flap	Northrop
737 spoiler flap	Boeing
JT9D 1/4 scale fan exit case (test)	Pratt and Whitney
Pressure vessels	Irad
Jet engine guide vanes (test)	Irad
Cylindrical tubes	Irad
Truss assembly on Applications Technology Satellites (ATS) models F and G	Fairchild/NASA
Light weight-high temperature all graphite honeycomb sandwich panels for space shuttle application (proposed)	NASA
Side braces and torque arms for A-37B main landing gear (test)	Bendix/AFFDL
A-7 speed brake	LTV
F-15 elevator structure (proposed and being tested)	McDonnell/Douglas
F-16 tail assembly, 2000 lbs of GECM proposed	General Dynamics
B-1 tail surfaces proposed-in testing phase	North American Rockwell

Table I. Aerospace Structures Fabricated or Proposed for Fabrication from Graphite Epoxy Composite Material

II. Theory

Basic Galvanic Corrosion Theory

Two dissimilar metals in a corrosive environment usually have a potential difference. A connection of these metals through a metallic circuit or by contact with each other causes electron flow between them due to this potential difference (Ref 6:29).

Basic corrosion textbooks describe galvanic corrosion as one of the primary forms of corrosion and discuss its cause, control, and prevention (Refs 1:8; 6:29). Ideas taken from basic sources that are pertinent to this investigation are the electrochemical reactions of corrosion and the application of Faraday's Law to relate current to material loss.

Galvanic corrosion is an electrochemical process in which an oxidation-reduction reaction occurs. The anode is the electrode where the oxidation half of the oxidation-reduction reaction takes place. Similarly, the reduction half of the reaction takes place at the cathode. When corrosion takes place, the oxidation half-cell reaction is

$$M \rightarrow M^{+n} + ne^{-} \tag{1}$$

where M is a metal, n is the metals valence for the reaction, and e has its usual meaning. It is apparent that electrons are provided for the galvanic current, and that the metal is undergoing dissolution into its ions. Several half-cell reduction reactions can take place on the cathode, but the one of particular interest to this experiment is the reduction of oxygen in a neutral or alkaline solution. This half-cell reaction is

$$O_2 + 2H_2O + 4e^{-} \rightarrow 4OH^{-} \tag{2}$$

This reaction will be discussed in more detail later in this section when

the subject of the cathodic behavior of graphite is addressed.

In this investigation, the measurement of galvanic current is used to predict galvanic corrosion trends. The relationship that converts galvanic current into metal dissolution or corrosion is Faraday's Law. This law states that one equivalent weight of metal or alloy is dissolved by the flow of one Faraday (96,500 amp-sec):

$$\text{Weight of metal reacting} = kIt \qquad (3)$$

where I is the galvanic current in amperes, t is the time of test in seconds, and k is a constant comprised of the equivalent weight of the metal divided by Faraday's Constant (Ref 1:6). Faraday's Law is the basic electrochemical relationship by which data collected in this study are converted into weight-loss and hence into corrosion rate.

EMF and Galvanic Series

Potential difference between metals based upon steady state reversible (non-corroding) conditions form a widely used but often misleading method for estimating galvanic corrosion. This method involves the use of the standard Electromotive Force (EMF) series which is defined as the potential that exists between metals immersed in a solution containing one gram atomic weight of their respective ions reference against the standard hydrogen electrode. Potential difference between two pure metals can then be calculated simply by determining the absolute difference in their EMF potentials.

A better method for estimating galvanic corrosion is the galvanic series. This method of predicting galvanic corrosion ranks various metals and alloys in a specified corrosive environment. Potential measurements are collected for the alloys of interest, and those with higher potential

differences are considered to be more prone to galvanic attack, whereas those alloys having similar potentials would be less apt to corrode galvanically. In the past, a frequently used rule for applying a galvanic series in corrosion estimates was that if the potential difference of two dissimilar metals in a given medium is less than 0.25 volts, then the alloy couple is compatible. However, the galvanic series has been abused in application over the years. Potentials vary with temperature, time, oxidizers in solution, and many other parameters. Therefore, extrapolation of data taken from one environment to one only slightly different can drastically change corrosion rates even to the degree that there is a cathode anode reversal.

A galvanic series is based upon a system in which the reactants are not at unity activity as is the EMF series. If unit activity does not exist, the Nernst equation is used to determine system potential (Ref 6:302). The Nernst equation can be derived from the Gibbs-Helmholtz free energy equation:

$$\Delta G_{P,T} = \Delta H - T\Delta S = -nFE \tag{4}$$

where $\Delta G_{P,T}$ is the free energy at constant temperature, ΔH is the change in enthalpy, T is temperature, ΔS is incremental entropy change, n is the number of electrons exchanged, F is the Faraday, and E is the cell potential (Ref 7:12). The Nernst equation states that:

$$E = E_0 + 2.3 \frac{RT}{nF} \log \frac{a_{oxid}}{a_{red}} \tag{5}$$

where E_0 is the standard half-cell potential, R is the gas constant, T is the absolute temperature, and a_{oxid} and a_{red} are the activities

of oxidized and reduced species, respectively. E, n, and F are defined above. The most important fact gathered from the Nernst equation is the sign of the free energy change since this determines the spontaneity of the redox reaction. In an electrochemical reaction, the most negative or active half-cell tends to be oxidized and the more noble half-cell tends to be reduced. Use of this principle for corrosion prediction states that corrosion will not take place unless the spontaneous direction of a redox reaction indicates oxidation. Thus EMF and galvanic series can determine unambiguously that corrosion will not occur. However, if the reaction indicates metal oxidation, corrosion may or may not occur.

Corrosion investigators are interested in the kinetics of corrosion (corrosion rates). Corroding systems are not at steady-state or equilibrium conditions; therefore, thermodynamic considerations cannot be reliably applied. In this study electrochemical methods are used to develop a galvanic series based upon kinetics or galvanic current data. An important concept used to analyze factors that control galvanic current and thus galvanic corrosion is the modern mixed electrode theory which is the basis for graphically depicting electrode kinetics.

Mixed Electrode Theory

In the above discussion galvanic corrosion was considered when comparatively large, relatively independent surfaces were used as cathode and anode. In this case, dissimilar electrodes exhibit a potential difference based upon the electrochemical properties of the entire surface of the respective electrodes. Thus the anodic reaction was considered to take place entirely on the anode, and the only reaction at

at the cathode was cathodic reduction.

It must be emphasized that all electrochemical corrosion, including uniform corrosion, can be said to take place through galvanic action. All the requirements for a galvanic cell can exist on the surface of any metal or alloy regardless of its noble nature; namely, a cathode, anode, metallic conductor, and an electrolyte. Localized microscopic cathodes and anodes exist on the electrode surface, and these anodic and cathodic areas continuously shift position. Contaminated moist environments provide the electrolyte and the metallic conductor exists because of intimate contact of grains at the grain boundaries. These localized galvanic cells are thus responsible for the uniform corrosion of metals and alloys.

When the localized electrochemical or galvanic cell is short-circuited, and net oxidation and reduction processes take place at the electrode interfaces, the potentials of the anode and cathode are no longer at their equilibrium potential (Ref 6:306). This displacement from the steady state potential is called polarization. Polarization is defined as the displacement of electrode potential resulting from net current. Polarization magnitude is often referred to as overvoltage, η, and is a measure of polarization with respect to the equilibrium potential of an electrode.

The Nernst equation (Eq 5) defines the equilibrium potential. Associated with this potential is the so-called exchange current density, which exists due to the localized anodic-cathodic reaction rate. Since no current flows at equilibrium, exchange current density is a misnomer. The relationship between exchange reaction rate and current density is:

$$r_{oxid} = r_{red} = \frac{i_0}{nF} \tag{6}$$

where r_{oxid} and r_{red} are the equilibrium oxidation rates and i_0 is the exchange current density. F and n have been previously defined. The magnitude of exchange current density is a function of several variables including (1) the particular redox equation, (2) the electrode composition, (3) temperature, and (4) the ratio of oxidized species to reduced species that are present. Exchange current density must be determined experimentally.

Electrochemical polarization is divided into two main groups which are activation and concentration polarization. Activation polarization is an electrochemical reaction controlled by a slow step in the reaction sequence. The Tafel equation describes overvoltage for activation polarization, and has a linear plot on semi-log graph paper:

$$\eta_a = \pm \beta \text{ Log } \frac{i}{i_0} \tag{7}$$

where η_a is the overvoltage, β is the Tafel slope, i is the rate of oxidation or reduction, and i_0 is the exchange current density.

Concentration polarization refers to electrochemical reactions which are controlled by the diffusion of a reaction species in the electrolyte. The limiting diffusion current density i_L, which is the maximum reduction rate for a given system is:

$$i_L = \frac{DnFC_b}{X} \tag{8}$$

where i_L is the limiting diffusion current density, D is the diffusion coefficient of the reacting ions, C_b is the concentration of the reacting ions in the bulk solution, and X is the diffusion layer thickness. Thus i_L is a function of diffusion coefficient, concentration of the reacting ions in solution, and diffusion layer thickness. The diffusion

layer thickness is influenced by electrode shape, system geometry, and agitation. Agitation tends to decrease the diffusion layer thickness because of convection currents thus increasing the limiting diffusion current.

If there is no activation polarization, the equation for concentration polarization is:

$$\eta_c = 2.3 \frac{RT}{nF} \text{Log} \left(1 - \frac{i}{i_L}\right) \tag{9}$$

where the terms have been previously defined. A graphical representation of Equation (9) is shown in Figure 1. Overvoltage is infinite at the limiting diffusion current. Figure 2 shows that if such variables as solution velocity, concentration, or temperature are increased, i_L is also increased.

Both activation and concentration polarization usually occur at an electrode and total overvoltage η_T is equal to the sum of η_a and η_c. Overvoltage due to concentration polarization is not a factor in anodic dissolution. The kinetics of the anodic dissolution is then simply the Tafel equation

$$\eta_{diss} = \beta \text{Log} \left(\frac{i}{i_0}\right) \tag{10}$$

The overall reaction for a reduction reaction on the cathode such as the reduction of hydrogen or, as in this case, the reduction of oxygen, is given by:

$$\eta_{red} = -\beta \text{Log} \frac{i}{i_0} + 2.3 \frac{RT}{nF} \text{Log} \left(1 - \frac{i}{i_L}\right) \tag{11}$$

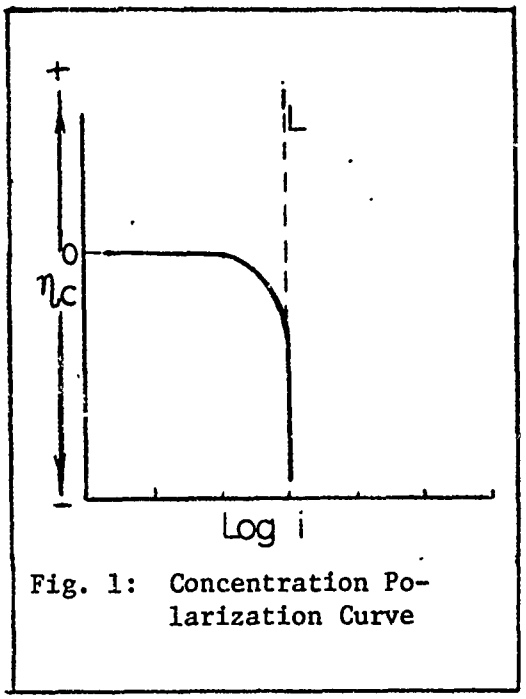

Fig. 1: Concentration Polarization Curve

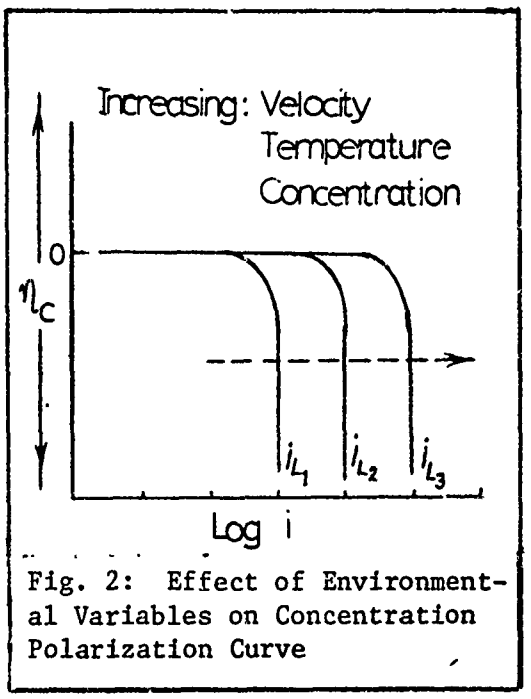

Fig. 2: Effect of Environmental Variables on Concentration Polarization Curve

This equation is graphically illustrated in Figure 3. It is seen that with three basic parameters, β, i_0, and i_L, the kinetics of virtually all corrosion reactions can be described. Equations (10) and (11) are the basic equations upon which mixed potential theory is based.

With these two equations, and the following two simple hypothesis, mixed potential theory can be applied to corrosion reactions. First, any electrochemical reaction can be divided into two or more partial oxidation and reduction reactions. Second, there can be no net accumulation of electrical charge during an electrochemical reaction (i.e., electrical charge is conserved). During the corrosion of an electrically isolated metal sample, the total rate of oxidation must equal the total rate of reduction (Ref 6:314).

If two metal surfaces comprise a local corrosion cell, one surface tends to be anodic, and involves a reaction between metal and metal ions.

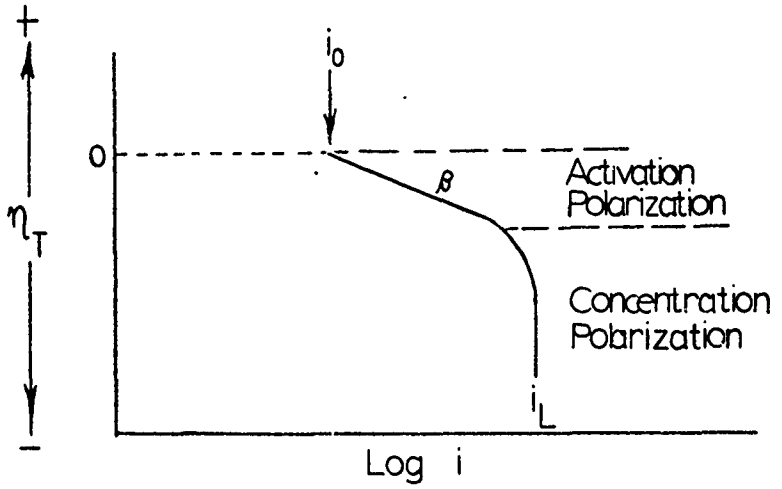

Fig. 3: Combined Polarization Curve - Activation and Concentration Polarization

The other surface tends to be cathodic, and reduction of either hydrogen ions or oxygen usually takes place. By the first hypothesis of mixed potential theory, each surface has a corresponding current exchange density i_{0a} and i_{0c}, and corresponding equilibrium potentials E_a and E_c. Metal and metal ions are in equilibrium at the anodic surface; for example:

$$Zn \rightleftharpoons Zn^{++} + 2e^- \qquad (12)$$

At the cathodic surface, for an acid solution, hydrogen will be in equilibrium with its ions:

$$2H^+ + 2e^- \rightleftharpoons 2H \rightleftharpoons H_2 \qquad (13)$$

The first hypothesis states that these partial oxidation and reduction reactions may be summed up to form the resulting corrosion cell reaction. The partial reactions shown in Figures 4 and 5 may then be combined to

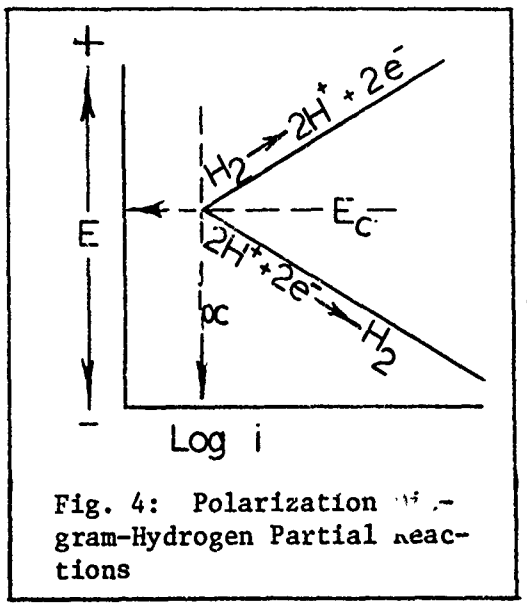

Fig. 4: Polarization Diagram-Hydrogen Partial Reactions

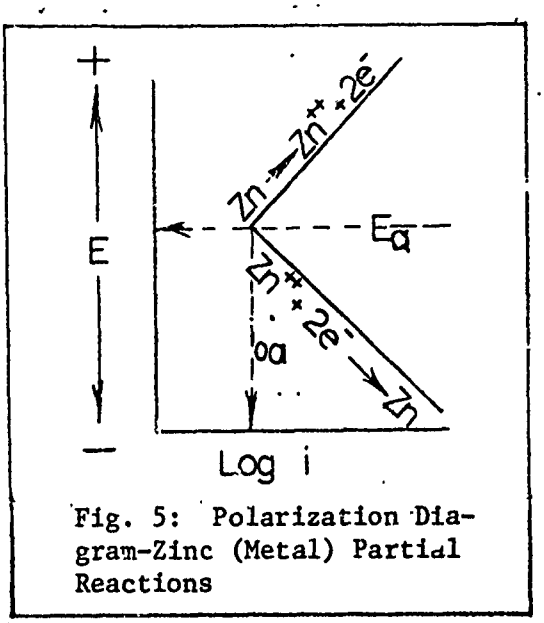

Fig. 5: Polarization Diagram-Zinc (Metal) Partial Reactions

form the total cell reaction graphically illustrated in Figure 6. The point at which the oxidation and reduction rates are equal determines the characteristic E_{corr} and i_{corr}. This occurs at the point of E_{corr} and i_{corr} intersection. The resulting corrosion density, i_{corr}, is the metal ion dissolution rate; i.e., the uniform corrosion rate of zinc in the acid solution.

The above example is a simple case illustrating the use of mixed potential theory. The linearity of both the cathodic and anodic half-cell reactions indicate that the reaction is under activation control. Curves that graphically represent half-cell potential as a function of current flow are called polarization curves or Evans diagrams (Ref 8:1291). The application of these curves can be used to show the type of control exhibited by local corrosion cells (Ref 9:486). Figure 7 is a schematic of the four basic types of control. When polarization occurs predominantly on the cathode, the cell is said to be under cathodic control. When

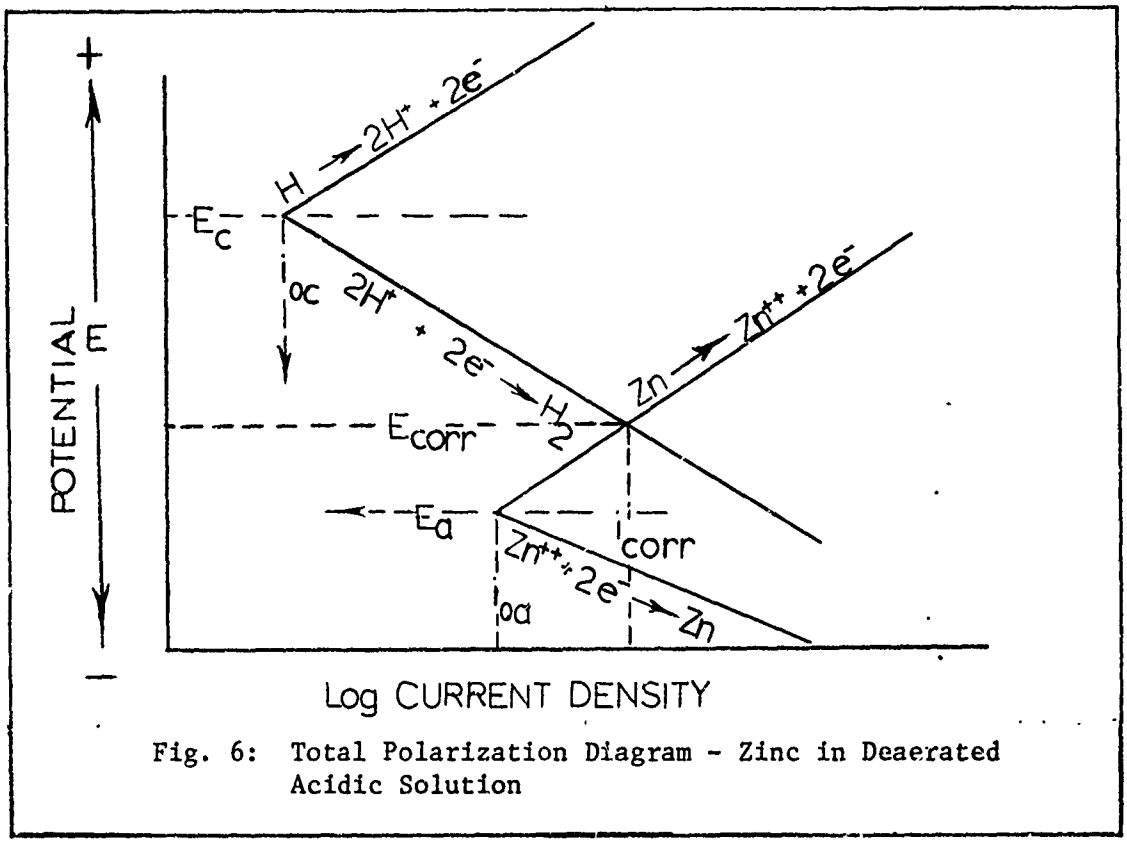

Fig. 6: Total Polarization Diagram - Zinc in Deaerated Acidic Solution

polarization occurs mostly at the anode, the reaction is referred to as being under anodic control. Mixed control occurs when both electrodes become approximately equally polarized. Resistance control occurs when the electrolyte resistance is so high that neither the anode or cathode is appreciably polarized.

In the above examples, only activation polarization at both anode and cathode was considered to illustrate effects of anode and cathode on polarization control. The shapes of the polarization curves are, however, most usually not linear. The shape of an Evans diagram is determined by many factors, such as the type of polarization, temperature, fluid agitation, surface film formation, electrolyte composition and conductivity.

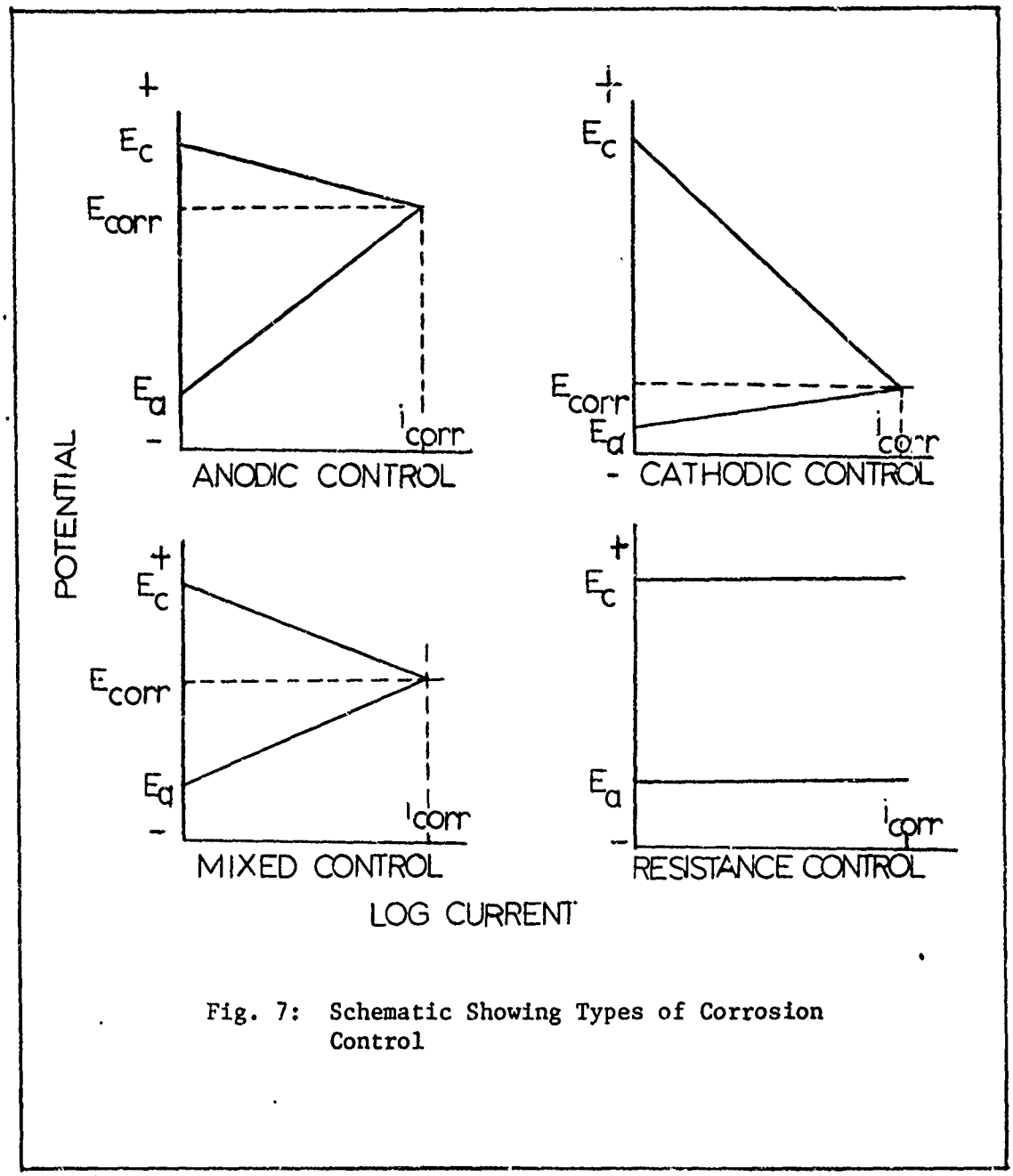

Fig. 7: Schematic Showing Types of Corrosion Control

Variables Affecting Uniform Corrosion

The rate of anodic dissolution of a metal may vary according to existing electrochemical and environmental factors. Several electrochemical factors affect electrode kinetics. But, as noted previously, activation and/or concentration polarization effects are the dominant rate determining factors in reaction rate control. Another important

electrochemical factor is passivity. Passivity is the loss of chemical reactivity (decreased corrosion rate) of a given metal surface under certain environmental conditions (Ref 6:16). Increased polarization of the anode surface toward more noble potentials results in an initial increase in anodic current density, then a decrease to a low essentially constant value independent of applied potential. Fig. 8 is an idealized anodic polarization curve typical of a metal that exhibits active-to-passive behavior. Note the very low corrosion current density in the passive region is indicative of a low corrosion rate. Passivity is due primarily to the formation of surface films that form a barrier that retards the oxidation or anodic dissolution reaction. Passivity is very sensitive to such factors as agitation, temperature, and oxidizer concentration.

Fig. 9 shows a metal that is active anodically and undergoes concentration or diffusion controlled polarization in the noble direction. As shown previously in a concentration controlled reaction, increasing velocity (agitation), temperature, and oxidizing agents in the electrolyte increases the limiting current density and thus the anodic corrosion rate.

Consider now a system under concentration polarization control,

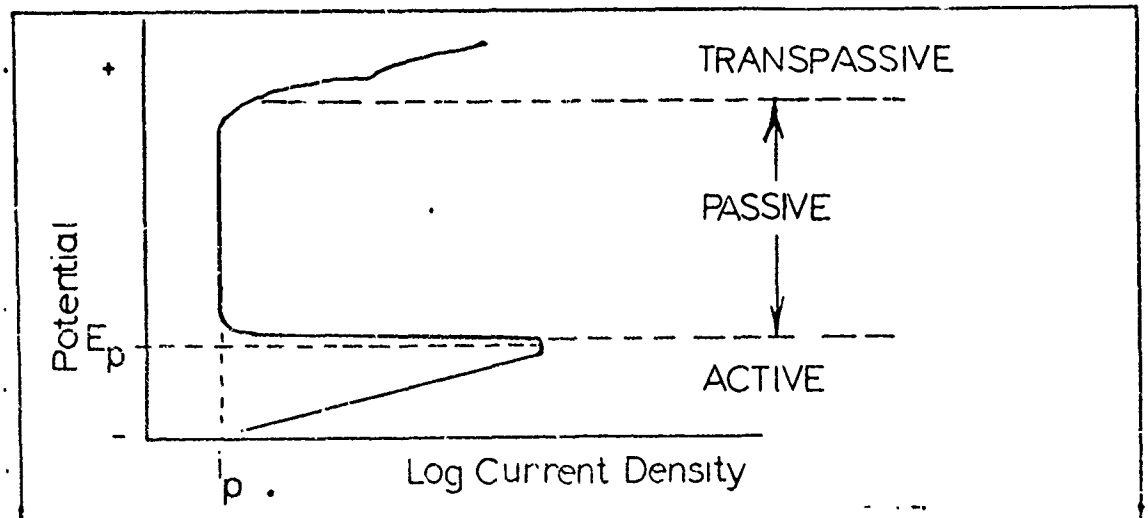

Fig. 8. Polarization Curve of Alloy Exhibiting Active-to-Passive Behavior

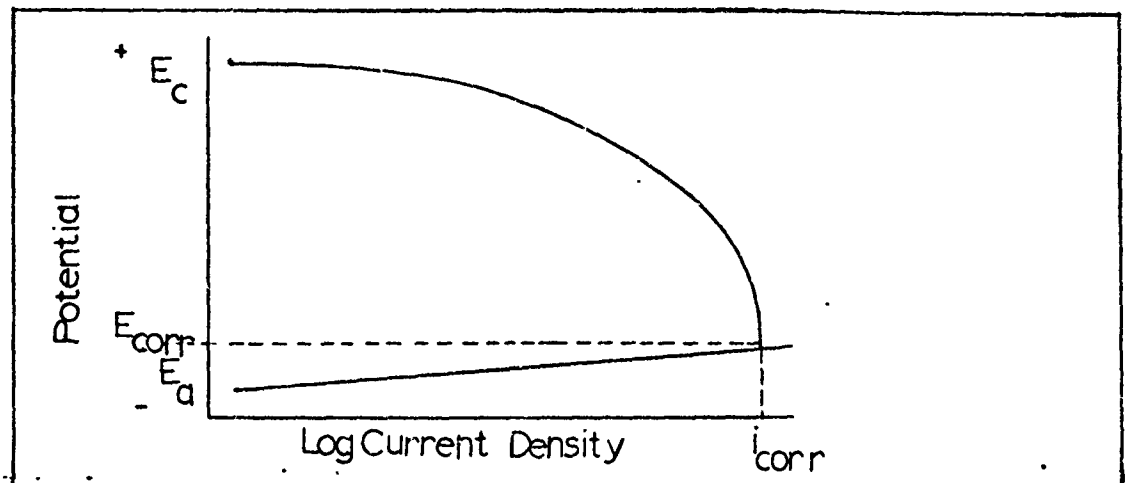

Fig. 9. Polarization Curve of Alloy Exhibiting Active Anodic Behavior and Concentration Control at Cathode

in which the metal surface exhibits active to passive behavior as indicated in Figure 10. Note that for the cathodic diffusion reaction curve A, the system is unstable because it intersects the anodic active-to-passive polarization curve at three points, and the reaction rate can oscillate active to passive with very slight changes in potential. Curve B represents an ideal situation, where the passive behavior of the metal surface greatly reduces corrosion rate since the limiting current density is beyond the nose of the anodic polarization curve. In this case, aeration or the increase in oxidizer concentration will increase the limiting current density thus decreasing the corrosion rate of the system. Agitation and increased temperature tends to move both curves to the right, thus increasing the charge transfer reaction whether the metal is active, passive, or in an unstable state.

In this study, concentration polarization is assumed since the cathodic reaction taking place in a neutral solution is the reduction of oxygen. Alloys tested in this research exhibit either activation

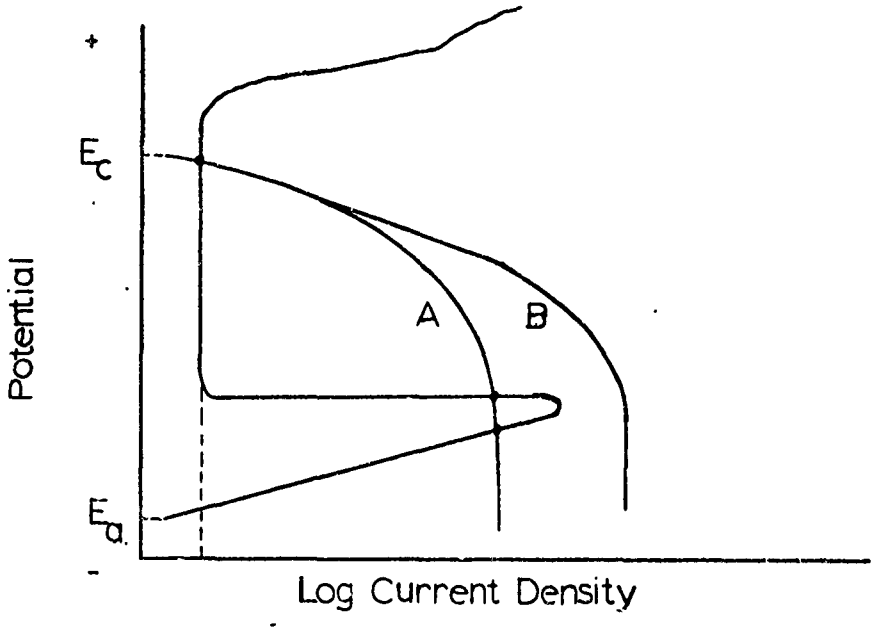

Fig. 10. Polarization Curve of an Alloy Exhibiting Active -to-Passive Anodic Behavior with Concentration Polarization of the Cathodic Reaction

control when anodically polarized, as in Figure 10, or exhibit an active-to-passive anodic polarization curve as in Figure 11. The cathodic reaction on the alloy surfaces is concentration controlled (i.e., the cathodic reduction of oxygen). For this research, temperature, electrolyte agitation, and aeration are maintained constant.

With the use of mixed potential theory, polarization diagrams, and other principles basic to the uniform corrosion on a metal or alloy surface, it is now convenient to investigate the effects associated with the galvanic coupling of a dissimilar metal to the alloy surface.

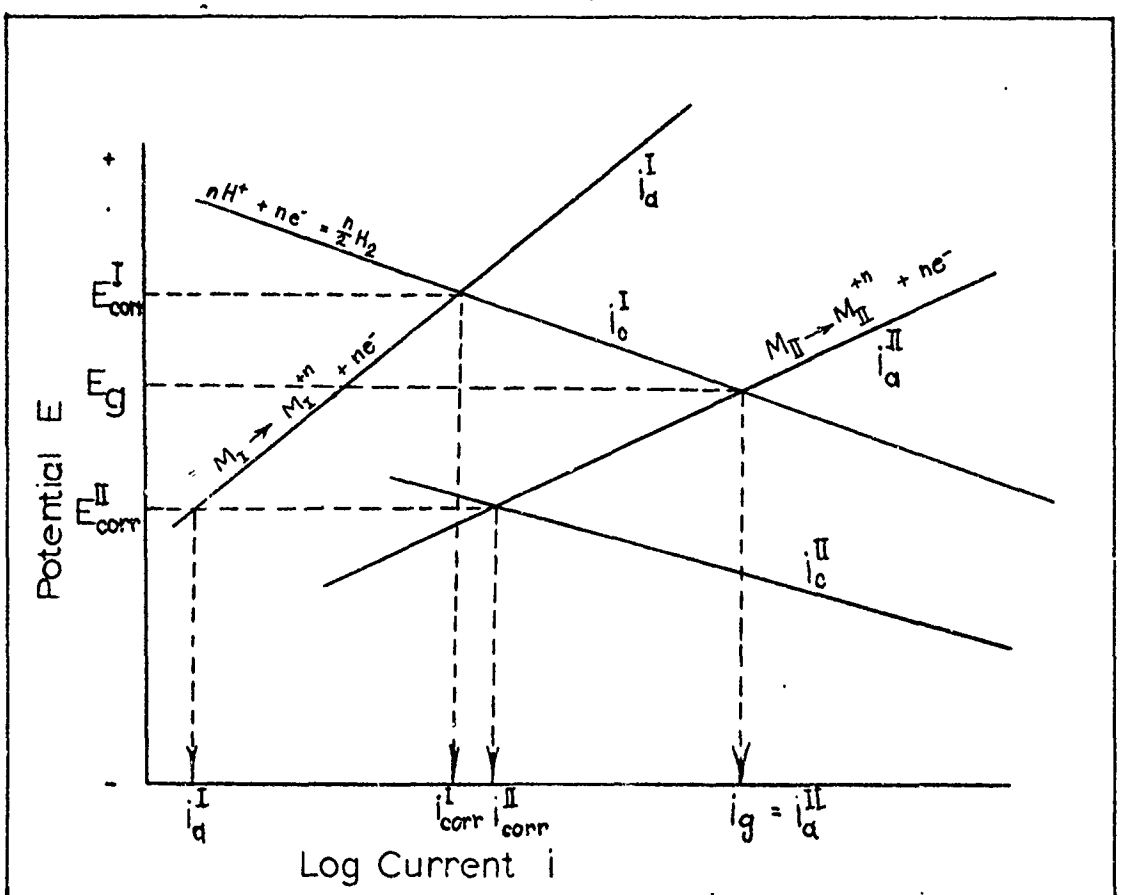

Fig. 11. Polarization Curve of Hypothetical Galvanic Couple in Acidic Solution Showing Galvanic Coupling Polarization Effects (Ref 10)

Galvanic Coupling

Polarization Effects. The principle of galvanic corrosion can best be shown by the use of polarization curves or Evans diagrams, where the polarization curves of each dissimilar metal or alloy are coplotted (Ref 10:139) as shown in Figure 12. This curve represents galvanic corrosion in an acid medium. Metal I has a more noble corrosion potential, E^I_{corr}, while Metal II has a more active potential E^{II}_{corr}. The respective currents are i^I_{corr} and i^{II}_{corr}. When coupled together, they are at the same potential E_g which is defined as galvanic potential. At this potential the main reaction at the surface of

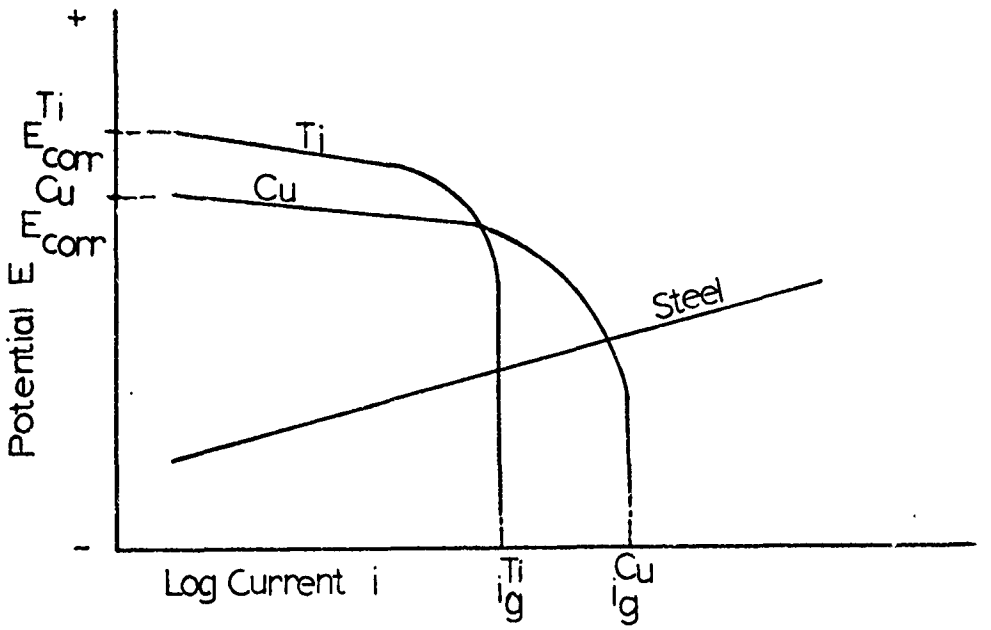

Fig. 12. Polarization Curves Showing Galvanic Current When Steel is Coupled to Titanium or Copper (Ref 10)

Metal I is hydrogen evolution, while the main reaction on Metal II is anodic dissolution. The reduction current i_c^I is equal to the metal oxidation current i_a^{II} and i_g the galvanic current:

$$i_c^I = i_a^{II} = i_g \tag{14}$$

The result of galvanic coupling is that the dissolution current, and thus the corrosion rate of Metal II is increased from i_{corr}^{II} to i_a^{II} at the same time that the dissolution current of Metal I is decreased from i_{corr}^I to i_a^I . Metal I is thus protected by an apparent increase in nobility (cathodic protection), whereas Metal II corrodes more rapidly. Different values of i_g can result for two metals with identical values of E_{corr}^I and E_{corr}^{II} because of their having different polarization curve slopes. Note that a galvanic series would have predicted such a couple to be very compatible, but as mentioned before,

polarization effects altered predicted behavior.

Titanium coupled to carbon steel tends to cause less acceleration of corrosion than coupling steel to copper in seawater where corrosion of metals is usually under concentration polarization control at the cathode. The polarization curve of steel coupled to both titanium and copper in seawater is shown in Figure 12. Notice that, although copper is nearer steel in potential E_{corr}, it accelerates the corrosion of steel more than titanium. The reason for this is that copper is a more effective electrode for the reduction of oxygen (limiting corrosion current density is increased) while the titanium alloy surface oxide film is an insulator to electron flow and thereby decreases the oxygen reduction rate. Predictions based upon potential differences alone (galvanic series) would have been invalid for this situation.

Area Effect. In addition to the effects of polarization, galvanic corrosion is dependent on the cathode-to-anode area ratio. The general rule in dissimilar metal design for atmospheric and marine use is to make the anode large compared to the cathode. Consideration of the fact that atmospheric and seawater corrosion polarization is under oxygen diffusion control makes this easily understood through the use of the Catchment Principle (Refs 10:142, 11:276). The Catchment Principle states that for an electrochemical reaction under concentration polarization control the anodic dissolution rate r_A is proportional to the ratio of the cathode-to-anode area A_C/A_A:

$$r_A = r_0 \left(1 + A_C/A_A\right) \tag{15}$$

where r_0 is the corrosion rate of the uncoupled anodic member of a galvanic couple. Note that as A_C increases:

$$r_A = r_0 \left({}^{A_C}/_{A_A}\right) \tag{16}$$

r_A becomes greater by a factor equal to the area ratio. On the other hand, for large A_A versus A_C, very little change occurs in r_A. Thus it is usually wise to avoid large cathode-to-anode areas. The application of the catchment principle requires that the alloy couple in question obey the principle.

Behavior of Graphite as an Oxygen Electrode

The property associated with the ability of a metal, or as in this case, GECM, to act as a substrate for the reduction of oxygen is an important concept to be emphasized in this research. This was shown in Figure 12 when steel was coupled to copper and titanium. Graphite has been used as a successful reversible oxygen electrode for many years (Ref 12:8). Because graphite is a good electrical conductor and because interfering oxide films such as those found on metals are not found on carbon surfaces, such a material as graphite makes a good inert electrode for the construction of oxygen electrodes (Ref 13:321). As demonstrated by Berl (Ref 14:263), the oxygen reduction on carbon electrodes in electrolytes containing added peroxide is reversible to the HO_2^- ions in neutral or alkaline solutions. Yeager (Ref 15:1057) suggests the following steps as a possible mechanism of the reduction

on carbon electrodes:

$$O_2 + H^+ + e^- \longrightarrow HO_2 \tag{16}$$

$$HO_2 + H^+ + e^- \longrightarrow H_2O_2 \tag{17}$$

$$H_2O_2 + 2e^- \longrightarrow 2OH^- \tag{18}$$

Comparison of these reactions with the single step oxygen reduction reaction given in Equation 2 indicates a different surface reaction mechanism on carbon electrodes. The intermediate step facilitates reduction of oxygen because it does not require breaking the oxygen bond. The above reaction is concentration controlled by the diffusion of dissolved oxygen to the electrode. Three basic ideas pertinent to this research are obtained from the above: (1) graphite is a good electrode for the reduction of oxygen, (2) a proposed reaction mechanism is listed, and (3) the reaction is controlled by diffusion of oxygen to the carbon electrode. The next step is to determine the validity of comparing a GECM electrode to a pure carbon electrode. The surface structure of graphite fibers is complex and matrix epoxy resins may introduce variables that further complicate the problem. Brown and Coomber (Ref 12:233) found that the polarization curve of GECM versus aluminum alloys was indeed controlled by diffusion or concentration polarization as indicated in Figure 13. Investigation of this curve shows that the aluminum is virtually unpolarized with almost all of the polarization occurring at the GECM electrode.

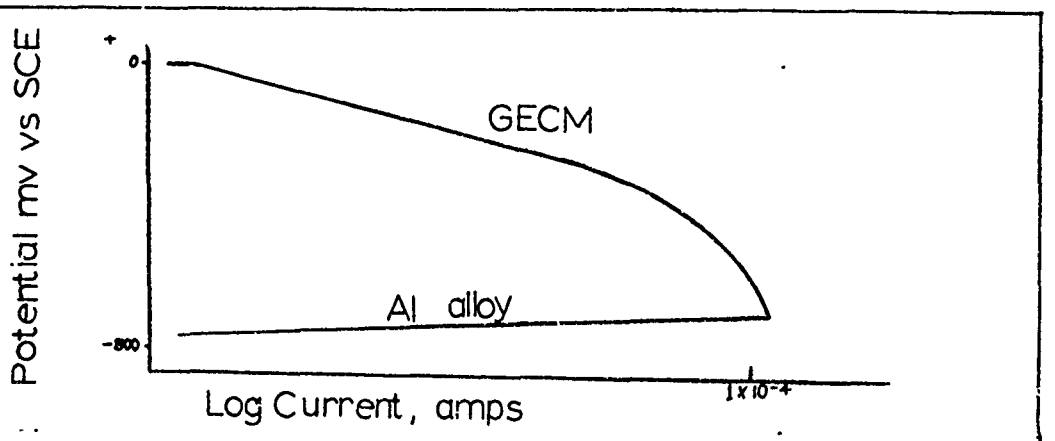

Fig. 13. Polarization Curve of Aluminum Alloy/GECM Couple (Ref 12)

Measurement of Galvanic Current

The increase in corrosion rate due to galvanic coupling is conveniently measured by monitoring the galvanic current flowing between the dissimilar alloys (Ref 10:143). Of the several methods used to measure galvanic current, the ZRA method has an advantage by allowing the galvanic current to be recorded continuously. Mansfeld and coworkers (Ref 10:143) used this technique to study galvanic corrosion of aluminum alloys used on aircraft coupled to other alloys in 3.5% NaCl as well as tapwater and distilled water. Results of these data were used to tabulate a galvanic series based on kinetic measurements of coupled metals rather than corrosion potential data. A typical curve of time versus galvanic current is shown in Figure 14. Here 2024 Al is the basic alloy tested with the dissimilar alloys indicated. The galvanic current versus time plots shown in the Appendices for CECM/alloy couples exhibit behavior similar to the typical time versus galvanic current plots of Mansfeld's 2024 Al/Alloy couples shown in Figure 14.

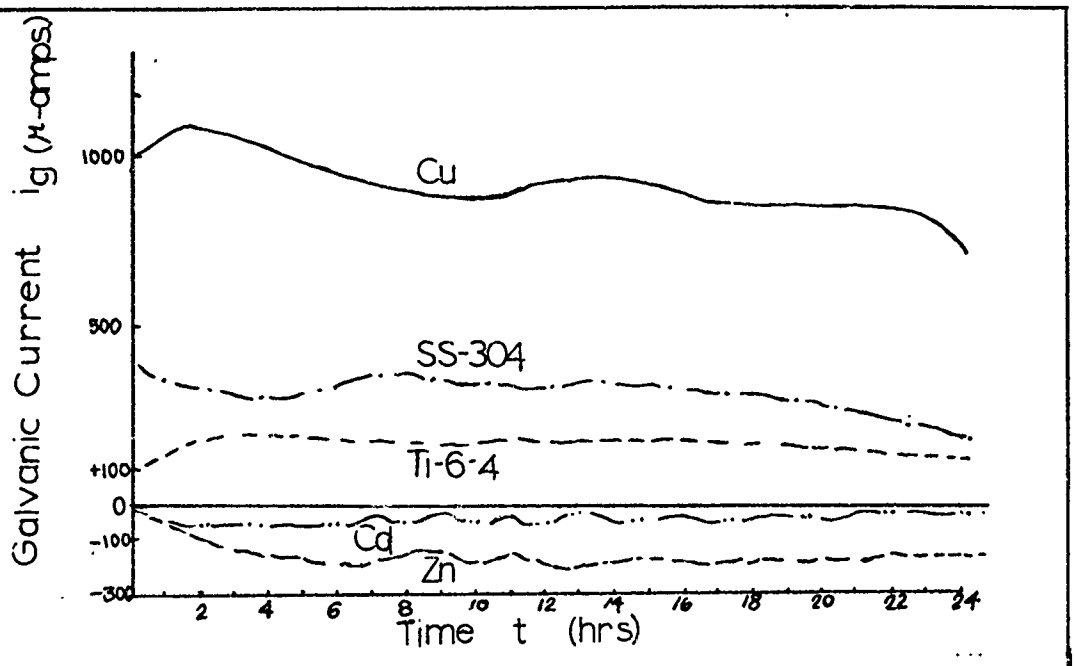

Fig. 14. Typical Plot of Galvanic Current vs. Time - Al 2024 vs. Indicated Alloys in 3.5% NaCl Solution (Ref 10)

Previous Studies of GECM/Alloy Couples

Fischer and DeLuccia (Ref 16:1) conducted electrochemical tests to determine the nature of galvanic corrosion when GECM is coupled to aluminum, steel, and titanium alloys in 3.5% NaCl solution. Approximately one volt potential difference was found between the composite and 7075 T6 and 7075-T651 aluminum alloys. This relatively large potential provided the driving force for a high corrosion of aluminum. The potential difference for Ti 6Al-4V and the composite was about 0.3 volt as received and 0.5 volt for a freshly polished surface. Corrosion current data showed that aluminum alloys, cadmium plated steel, cadmium plated steel plus chromate conversion coat are much more reactive than Ti 6Al-4V when coupled to GECM (approximately 15 versus 0.002 μ-amp/cm^2). This technique provided a means of ranking the corrosion susceptibility when GECM

is coupled with various aircraft alloys.

Johnston and coworkers (Ref 5:1) also conducted electrochemical studies at GECM/Alloy couples. Electrochemical data in 3.5% NaCl solution included determining the corrosion potential of uncoupled GECM and various alloys (see Table II) versus Saturated Calomel Electrode (SCE) by the use of an electrometer (Figure 15).

Johnston also measured galvanic corrosion currents using the ZRA potentiostat method of electrochemical analysis. At pH = 7, air saturation, and one molar NaCl, the aluminum/GECM couple had a galvanic current of 400 μ-amp, the aluminum/iron couple was 200 μ-amp, and the aluminum/Ti 6Al-4V couple was 10 μ-amps at room temperature.

Electrochemical data derived by Brown and Coomber provided pertinent information for this research (Ref 12:232). Corrosion potential measurements were made on a variety of GEC materials in 5% aqueous NaCl. The GECM slowly reached an equilibrium potential, normally about 300 mv positive to SCE. No correlation of potential with the type of graphite fiber was found. Aluminum and aluminum alloys were found to be about 600-700 mv negative to SCE.

Polarization studies showed that for GECM/aluminum alloy couples, the polarization occurs almost exclusively at the GECM. The effects of chloride ion concentration, pH, temperature, oxygen concentration, and nature of cations and anions were studied with the following results: (1) the pH of the aqueous salt solution has little effect on polarization between pH 3 and 11, (2) rate of attack increases with temperature, but over the range of temperatures commonly found on aircraft components, the acceleration should not be of concern, (3) concentration of NaCl has only a small effect. It was noted that a serious corrosion risk at

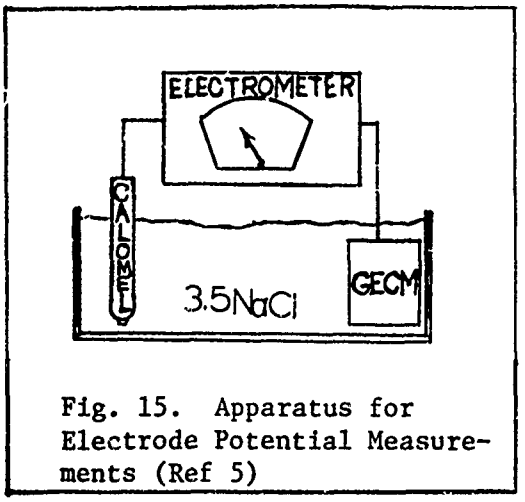

Fig. 15. Apparatus for Electrode Potential Measurements (Ref 5)

Material	E_{corr} (mv)
GECM	+ 120
Ti 6-4	- 420
4340 Steel	- 600
Al 7075 T6	- 780

Table II. Uncoupled Potentials vs. SCE Determined by Johnston et al (Ref 5)

GECM/aluminum alloy couples exist due to galvanic attack with GECM acting as a noble metal. Stated also was that GECM acts as an oxygen electrode and the rate of attack on the aluminum was proportional to the oxygen concentration in the electrolyte.

III. Experimental Procedure

Materials

Graphite-epoxy composite materials tested in this study are listed in Table III, along with a short description of the material, its manufacturer, and the number of samples tested.

Alloys tested and their nominal composition in weight percent are listed in Table IV. Experimental alloys that have been proposed for aerospace application are Al 2020-T651, MA-87, Aluminum Graphite (Al-Gr), 10 Ni Mod steel, and AFC-77 stainless steel. Since very little corrosion testing has been accomplished on these alloys, the corrosion potential and galvanic current data collected in this research should be of particular interest.

Graphite Material	Manufacturer	Description	Number Tested
AS/3501-5	Hercules	Amine-cured epoxy resin reinforced with unidirectional graphite fibers, designed to withstand temperatures up to 350°F.	44
Modmor	Narmco	Composed of layered 5206 tape with a modified epoxy resin system	5
Magnamite	Hercules	Hercules AS fibers in an epoxy E-298 matrix	2
T-300	Thornel	Graphite fibers impregnated with an epoxy specified as 5208.	4
Pure Graphite	———	———	5

Table III. Graphite Epoxy Composite Materials (GECM) Tested, Manufacturer, Short Description, and Number Samples of Each Tested, Along with Pure Graphite

Test Alloys	Nominal Composition, Weight %
Al 2020 T651	4.5 Cu, 1.0 Li, 0.5 Mn, 0.2 Cd ---- Al
Al 7075 T6	5.6 Zn, 2.5 Mg, 1.6 Cu, 0.3 Cr ---- Al
MA-87 (P/M)	6.5 Zn, 2.5 Mg, 1.5 Cu, 0.4 Co ---- Al
AL 2024 T6, T3	4.5 Cu, 1.5 Mg, 0.6 Mn ---- Al
Al Graphite	30.0 Graphite, 60.0 Al 6061 --- 1.0 Mg, 6.0 Si, 2.5 Cr, 2.25 Cu --- Al
4340 Steel	0.42 C, 0.75 Mn, 0.25 Si, 1.85 Ni, 0.82 Cr, 0.25 Mo, --- Fe
300M Steel	0.42 C, 1.85 Ni, 0.9 Cr, 5.0 Mo, 1.6 Si, 0.85 Mn --- Fe
10% Ni Mod Steel	2.0 Cr, 10.0 Ni, 14.0 Co, 1.0 Mo, 0.14 C --- Fe
4130 Steel	0.42 C, 0.95 Cr, 0.2 Mo, ---- Fe
1020 Steel	0.2 C ---- Fe
SS-440C	17.0 Cr, 0.5 Mo, High C --- Fe
SS-301	18.0 Cr, 8.0 Ni --- Fe
SS-304	19.0 Cr, 10.0 Ni, Low C --- Fe
SS-PH 17-7	.07 C, 17.0 Cr, 7.0 Ni, 1.2Al --- Fe
SS AFC-77	0.15 C, 14.5 Cr, 13.0 Co, 5.0 Mo, 0.4 V --- Fe
Inconel	15.0 Cr, 7.0 Fe, --- Ni
Inconel X	15.0 Cr, 7.0 Fe, 2.5 Ti, 1.0 Co, 0.7 Al, --- Ni
Rene' 41	19.0 Cr, 11.0 Co, 10.0 Mo, 3.0 Ti, 1.5 Al, --- Ni
Ti 6Al-4V	6.0 Al, 4.0 V, ----- Ti
Ti 6Al-2Sn.....	6.0Al, 2.0 Sn, 4.0 Zr, 2.0 Mo, ----- Ti
Be-Cu	1.74 Be ---- Cu

Table IV. Alloys Tested with Nominal Composition in Weight Percent

Equipment

Uncoupled Open-Circuit Potential and Potential Difference Measurements. Open-circuit potentials ϕ_{corr} for the uncoupled samples were determined by using the apparatus shown in Fig. 16. This is similar to the method used by Johnston (Ref 5:3) in which the electrometer is replaced by a digital voltmeter (DVM). The open-circuit potentials were measured using the saturated calomel electrode (SCE) as a reference electrode.

Potential difference, $\Delta\phi_{corr}$ between GECM and an alloy could be determined by two methods. The first consisted of finding the stabilized open-circuit values of ϕ_{corr} for each member of the couple and calculating the absolute difference. The second method was a direct measurement using the DVM across the couple terminals, and taking an instantaneous reading. The direct method was found to correspond with the calculated method, and was easier to implement when both samples were in the same test beaker as was the case in this experiment.

The only electronic equipment required for ϕ_{corr} and $\Delta\phi_{corr}$ measurements was the DVM. A Hewlett-Packard Model 3440A DVM with approximately 10 megohms input impedance was used in this experiment.

Galvanic Current Measurement. Galvanic current, i_g, can be measured by application of the potentiostat as a ZRA (zero resistance ammeter). In potentiostatic studies, the electrode referred to as the auxiliary or counter-electrode is, in this experiment, the cathodic or more noble member of the galvanic couple. GECM or pure graphite is this cathode. The working electrode is the anode, which is the coupled alloy. The reference electrode is a SCE.

The measurement of i_g requires that the magnitude of very small currents be measured without introducing current loss into the circuit

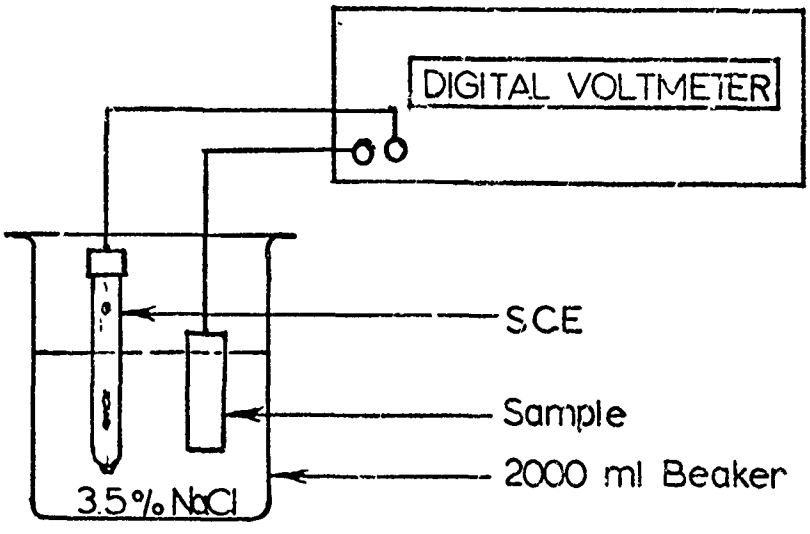

Fig. 16. Apparatus Used to Determine Corrosion Potential ϕ_{corr}

when the two electrodes are shorted together in the 3.5% NaCl electrolyte. The application of a normal current measuring device or recording instrument between the cathode and anode affects the characteristics of the cell producing inaccurate results (Ref 17:35).

The manually balanced ZRA overcomes this problem by using a controllable current from a separate source passed through the measuring ammeter in the opposite direction of that flowing in the electrochemical cell. It is possible to adjust the control current to a point where the potential drop across the measuring ammeter is zero. Under this condition, the effective impedance of the measuring device would likewise be zero, and the current flowing in the external circuit would be exactly equal to that flowing in the electrochemical cell. An important point to be noted is that the opposing current can be measured by various means without

changing the electrochemical properties of the galvanic cell. The method of using the potentiostat for galvanic corrosion current measurements in electrolytic galvanic cells was first discussed by Devay, Lenyel, and Meszaros in 1969 (Ref 18:157).

The method of connecting the potentiostat to the galvanic cell when the potentiostat is applied as a ZRA is shown in Figs. 17 and 18. Fig. 17 represents the galvanic cell by its electrical equivalent. With the reference voltage set at zero, the potentiostat operates as a single-ended-input-inverting amplifier where the reference electrode terminal R.E. is at virtual earth and is also a summing point.

Since the current i_f equals i_{in}, the cell current magnitude can be read directly on the potentiostat output ammeter. An alternate method and the method used by this researcher, is to measure i_f by measuring the output potential V_o between the working electrode W.E. and the auxiliary electrode A.E., and dividing this by the preset resistance value of the feedback resistor R_f.

Because the gain of the potentiostat and the output voltage V_o controls the error signal V_e, the smaller the output signal required for measurement, the nearer zero will be the error voltage V_e. For this reason, the value of R_f should be kept as low as possible compatible with the maximum current flow to be measured. A high input impedance recorder allows the change in galvanic current with time to be plotted.

The equipment required to set up the ZRA circuit described above was: (1) a potentiostat, (2) a DVM to set and monitor the potentiostat control voltage at 0.000 volts, (3) another DVM to monitor the external voltage V_o, (4) a decade resistance box, (5) a recorder with high input

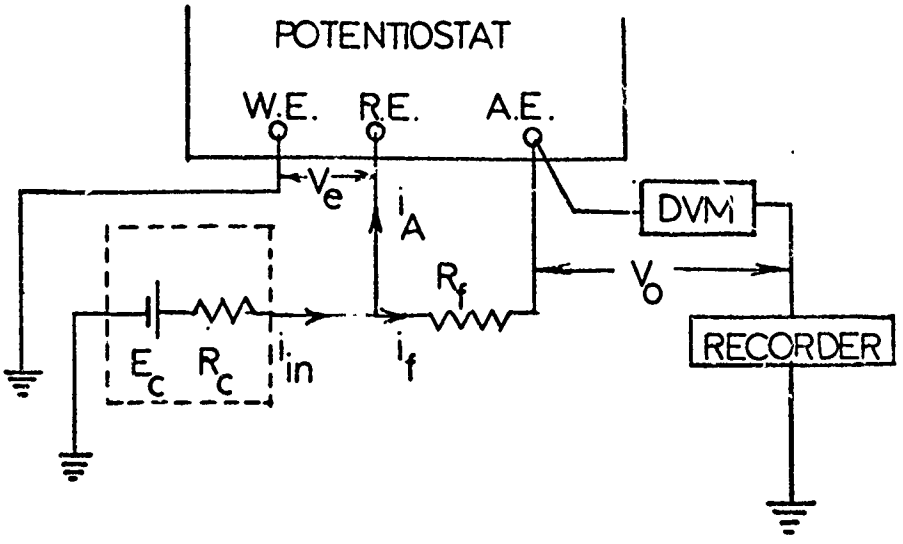

Fig. 17: Circuit Diagram of Potentiostat ZRA Used to Measure Galvanic Current with the Galvanic Cell Represented by Its Electrical Equivalent

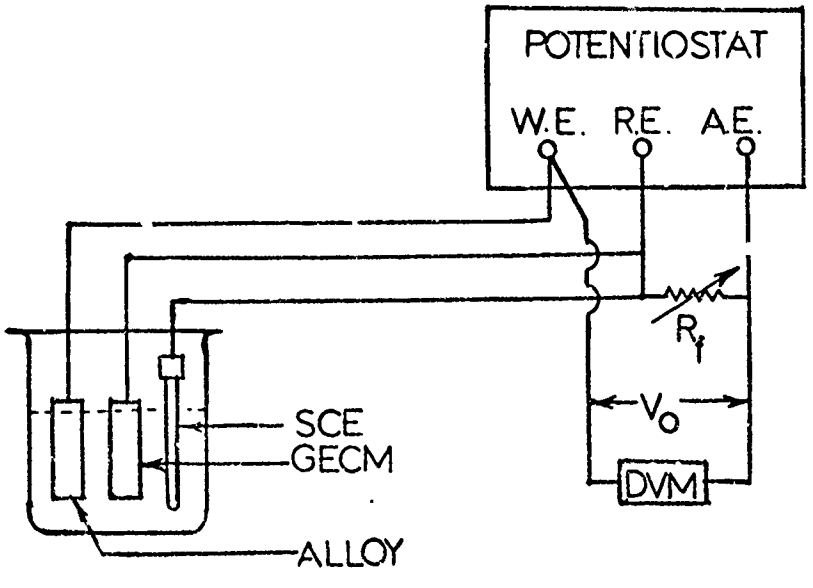

Fig. 18: Schematic of Potentiostat ZRA Used in Measuring Galvanic Current

impedance for recording external voltage V_o, and (6) electrical leads exhibiting minimum lead loss connecting the various electronic components indicated.

Two makes of potentiostats were used: (1) the Magna Model 4700M Electronic Potentiostat and (2) the Wenking Model 70HC3 Solid State Electronic Potentiostat.

Hewlett-Packard Model 3440A DVM's were used to both monitor control voltage and to indicate the external voltage V_o.

A Nesco Model JV170 Recorder with 10 megohms/volt input impedance was used to record V_o.

It is important to emphasize that the measurement of V_o is all that is required to obtain galvanic current i_g. By knowing R_f, which is preselected on the decade resistance box, an application of Ohms Law gives i_g:

$$i_g = \frac{V_o}{R_f} \tag{19}$$

The ranges of voltages V_o measured in this experiment were from 0 to 500 millivolts (mv). A 1000 Ω R_f provided the accuracy required for currents in the microamp (μ-amp) range. Thus, V_o and i_g could be read directly from the DVM and recorder since voltage magnitude in mv was identical to the current magnitude in μ-amps.

The Test Cell

The test cell used in this experiment is shown in Figure 19. The 2000 ml beaker was filled with approximately 1000 ml of 3.5% aqueous NaCl reagent. A polytetrafluoroethylene cover was provided to hold evaporation to a minimum. Holes in the cover were provided for leads

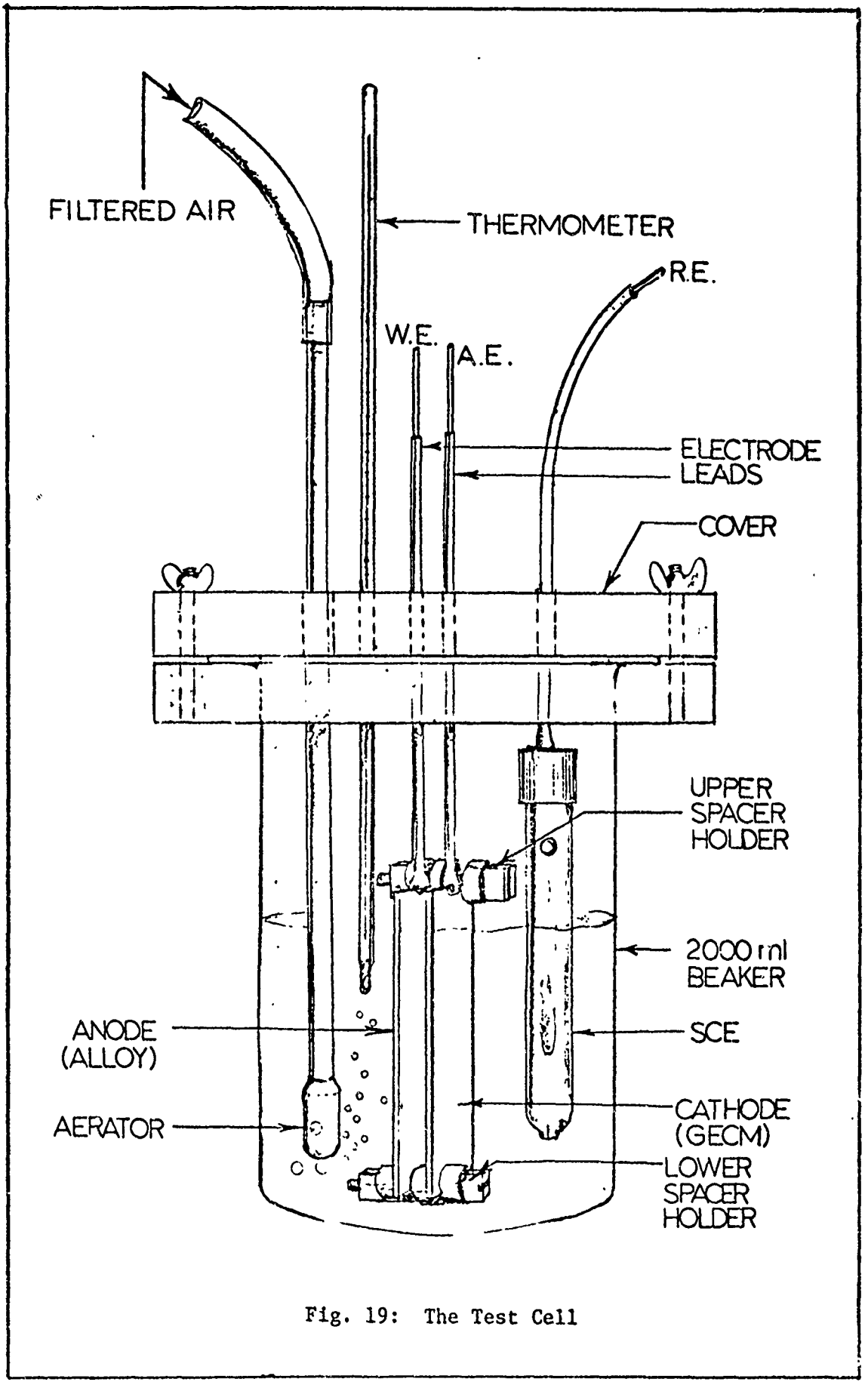

Fig. 19: The Test Cell

from the samples and reference electrode, a thermometer, and the aeration apparatus. The SCE and coupled samples were placed in the cell prior to securing the cover and the subsequent filling with electrolyte.

Specimen and Specimen Holder/Spacer Apparatus

The test samples were flat coupons 2.54 X 7.62 cm (1 X 3 inches) with variable thickness which did not exceed 0.635 cm (0.25 in) as shown in Fig. 20. Alloy surfaces were wet ground with 120 grit emery paper. GECM sample surfaces were tested in the as received condition without any use of abrasives.

Lead wires (#12 or #14 plastic-covered solid copper) were approximately 15 cm long (6 in) and were mechanically fixed to the sample by either of two methods. A fixed connection was chosen over the commonly used alligator clips because better contact could be made while eliminating current losses due to corrosion product build-up and accumulation of moisture at the lead-specimen interface. The first method (Fig. 20A) consisted of top drilling a sample to a 0.25 in depth and friction forcing the lead into the hole for good electrical contact. The second method was used for samples too thin to top drill. In this case, a hole was drilled through the sample, and the flattened drilled lead wire was bolted to the sample as shown in Fig. 20B. The lead-to-sample junction was then covered with epoxy to secure the joint. This was followed by top-coating with silicone elastomer to preclude moisture penetration and for electrical insulation.

The holder/spacer device consisted of two nylon bolts (electrically inert) with nylon nuts, washers, and an 0.32-cm (0.125 in) spacer to separate the GECM and alloy surfaces and to keep them parallel. One

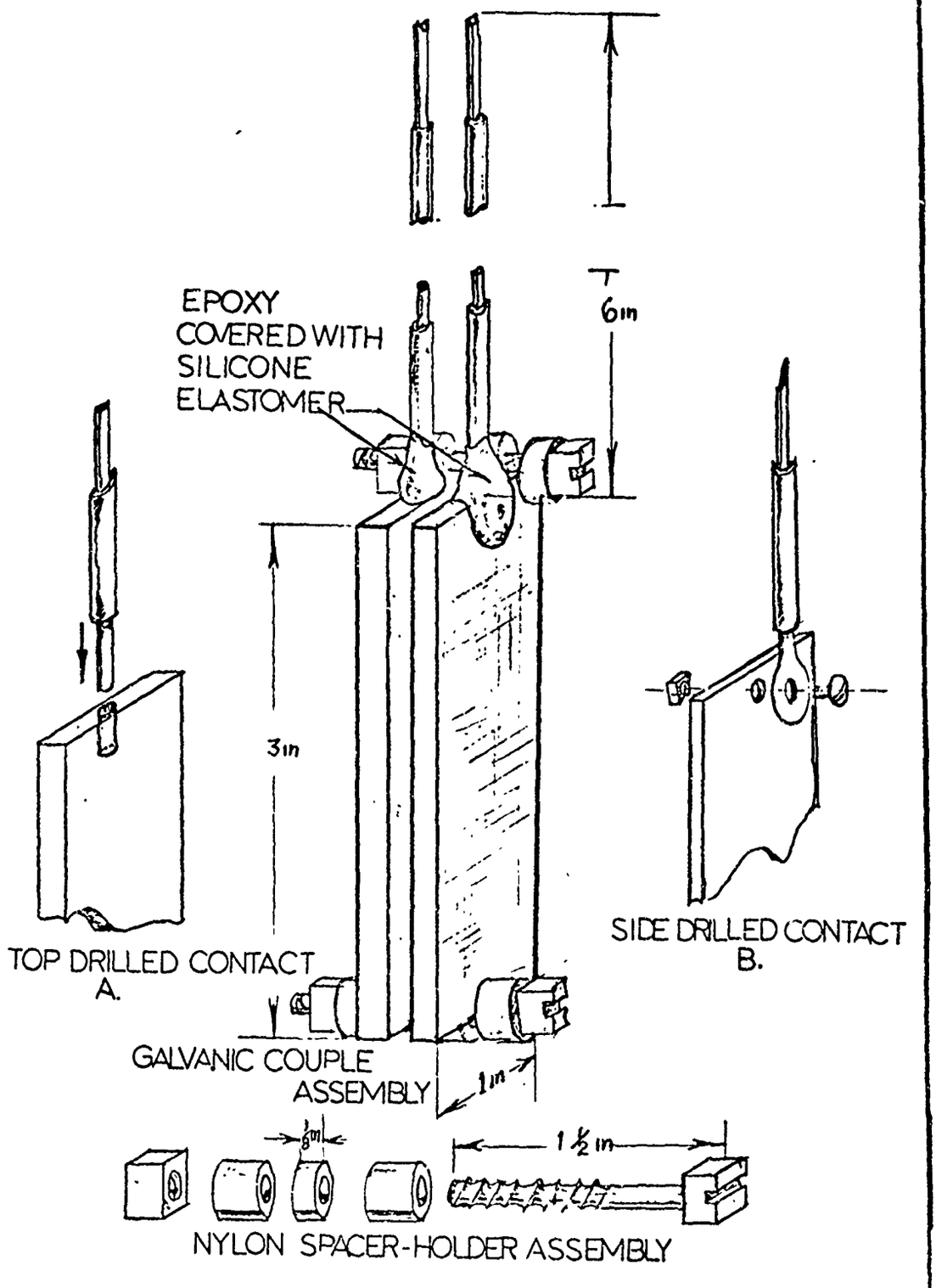

Fig. 20: Specimen Assembly for Galvanic Testing

bolt assembly was placed at the top of the sample and the other at the bottom. The bottom bolt prevented the samples from contacting the bottom of the test beaker. This spacer covers a very small area of couples total galvanic reaction surface, thus reducing the effects of crevice corrosion. Fig. 21 shows an assembled test couple ready to be placed in the test cell.

Experimental Technique

The following is a procedural outline of items accomplished during the completion of a test run.

Cleanliness is of major importance in corrosion testing. All test cell apparatus was washed in laboratory detergent and wetting agent, rinsed in warm tapwater, with a final rinse in distilled water and then allowed to air dry. Clean apparatus was handled with rubber gloves, tongs, or laboratory tissues.

Specimens were degreased using a 5 minute acetone soak. Alloys were not boiled in benzene, because of possible deterioration of the silicone elastomer connection sealant due to chemical reaction with benzene. The samples were then allowed to dry, and rinsed off with distilled water. A heat gun was used to drive off water.

The 3.5% NaCl solution was prepared in 1000 ml quantities by first partially filling a calibrated 1000 ml flask with distilled water, adding 35 grams of reagent-grade NaCl, then allowing the NaCl to dissolve. Distilled water was then poured into the flask to the 1000 ml calibrated mark. The pH of the NaCl solution was then taken and recorded using a standardized Beckman Zeromatic II pH meter.

Both samples were weighed to the nearest 0.1 miligram before and

after corrosion testing. This allowed the determination of a weight-loss or gain to be used as a comparison to that determined from galvanic current data. Weight-loss determination was not in accordance with ASTM procedure in that a chemical or electrolytic method was not used to remove corrosion residue (Ref 19:493). Corrosion product was removed from corroded samples using a rubber stopper and distilled water. This method is described by Fontana (Ref 6:119). It is admittedly inaccurate, but time was too limited to conduct exhaustive weight-loss tests. Weight-loss data, though imprecise, should indicate corrosion trends for comparison with data derived from galvanic current measurement. The electrochemical methods were of primary concern in this experiment.

The samples were then assembled in the holder/spacer, and placed along with the SCE in the test beaker. Electrical leads were guided through the cover and the cover was tightened to the beaker. The aerated 3.5% NaCl solution was then funneled into the beaker until the fluid level was about 0.25-in below the sample-to-lead junction on the coupled assembly. Fluid temperature was then recorded and aeration started in the test cell.

Before connection into the ZRA circuit, the uncoupled corrosion potentials of the couple members were monitored for 15 minutes, and recorded along with potential difference ($\Delta\phi_{corr}^{start}$) just before connection into the ZRA circuit.

Placing the potentiostat into "operate" activated the ZRA circuit, and galvanic current i_g was recorded over a 24 hour period. Immediately after test, ϕ_{corr}^{end} and $\Delta\phi_{corr}^{end}$ data were taken and this repeated 15 minutes later to determine polarization changes. Post test pH, and temperature were recorded. Samples were cleaned of corrosion residue,

dried, and reweighed. Test apparatus was cleaned and prepared for the next test run.

It was fortunate that test equipment existed for three complete experimental set-ups. This allowed many more couples to be tested especially when all equipment was operating properly. Also, due to the number of test cells, testing continued even when there was equipment failure. A large amount of data was collected over a relatively short period of time.

In order to show the reproducibility of a particular GECM/alloy couple, a minimum of two complete test cycles were performed for each couple. Also, because different types of GECM were tested on a random basis, additional runs were required. Tests were made with pure graphite for comparison purposes. A total of 56 tests were completed.

Data Reduction and Analysis

The recording plots of galvanic current, i_g, were graphically integrated to produce an average galvanic current $\bar{i}_g$. The data points used in determining $\bar{i}_g$ were programmed into a computer plotting routine to produce the galvanic current versus time plots shown in the Appendices. A computer program was used to reduce $\bar{i}_g$ data into average galvanic current density $\bar{i}_{gcd}$, weight-loss over the test duration (w.l.), and corrosion rates in miligrams per square-decimeter per day (m d d) and mils per year (m py). Parameters other than $\bar{i}_g$ required for data reduction were: (1) alloy equivalent weight, (2) alloy density, (3) specimen planar area, and (4) test duration. Tables VI through XI list the reduced electrochemical data.

Actual weight-loss data, test duration and the specimen area were

used to calculate the dissolution rates r_A of the test specimen in mpy. The r_A values are also listed in Tables VI through XI as a basis of comparison against values determined from $\bar{i}_g$ data.

IV. RESULTS, DISCUSSION, AND CONCLUSIONS

Results

Corrosion Potential Measurements. The start and end test corrosion potentials (ϕ^{s}_{corr} and ϕ^{e}_{corr}) are listed in Tables V and VI. Values of ϕ^{s}_{corr} for the alloys (Table V) are of interest because this list forms a galvanic series for aerated 3.5% NaCl solution at room temperature (22 $\pm$ 1 C) and neutral pH (7). The ranking in Table V lists the most noble alloy first, and descends in order to the most active alloy, or negative potential. As shown, stainless steels occupy the more noble potentials while aluminum alloys are most active. Data of this type are most often considered when there is a question of galvanic corrosion compatibility. It will become evident from galvanic current measurements that the use of potential differences determined from a galvanic series of this type is not a reliable method for estimating galvanic corrosion compatibility.

Comparing ϕ^{s}_{corr} and ϕ^{e}_{corr} of a given alloy suggests that the direction of potential change is indicative of the kinetic behavior of the alloy. It is noted, in general, that alloys with decreasing ϕ^{s}_{corr} versus ϕ^{e}_{corr} tend to have higher galvanic corrosion current than vice versa. For example, titanium alloys, nickel-base alloys, and most stainless steels have a ϕ^{s}_{corr} versus ϕ^{e}_{corr} that becomes more positive. These same alloys have low galvanic current. The opposite was true of most of the aluminum alloys and steels. These trends are closely related to the polarization effects or the kinetics of the galvanic reaction, and are thus more clearly shown when galvanic current is measured.

Table VI lists potentials for the graphite materials tested. The

Alloy	ϕ^{s}_{corr} (mv)	ϕ^{e}_{corr} (mv)
SS-301	-174 ± 65	-119 ± 76
Inconel X	-175 ± 25	-102 ± 10
SS-304	-210 ± 46	-109 ± 35
Be-Cu	-225 ± 5	-220 ± 5
PH 17-7	-252 ± 23	-139 ± 10
AFC 77	-318 ± 70	-209 ± 7
300M	-330 ± 5	-567 ± 4
Ti 6Al 4V	-343 ± 4	-270 ± 25
10 Ni Mod	-358 ± 30	-529 ± 18
Ti 6Al 2Sn 4Zr 2Mo	-359 ± 29	-217 ± 69
Inconel	-364 ± 100	-161 ± 57
SS-440C	-391 ± 7	-511 ± 32
Rene 41	-437 ± 110	-184 ± 84
4340	-534 ± 4	-667 ± 5
4130	-537 ± 55	-673 ± 10
1020	-543 ± 15	-566 ± 37
2024 T3	-652 ± 25	-783 ± 8
2024 T6	-656 ± 12	-753 ± 23
2020 T651	-724 ± 5	-821 ± 51
7075 T6	-775 ± 5	-751 ± 31
MA-8[illegible] '72)	-862 ± 3	-823 ± 7
MA-87 (73)	-868 ± 3	-849 ± 5
Aluminum Graphite	-868 ± 10	-808 ± 6

Table V. Corrosion Potentials Before (ϕ^{s}_{corr}) and After (ϕ^{e}_{corr}) Galvanic Couple Test, 3.5% NaCl Solution, pH-7, 22± 1°C

Graphite	ϕ_{corr} (mv)	ϕ^{s}_{corr} (mv	ϕ^{e}_{corr} (mv)
3501-5	+179	+145 high +9 mean -221 low	+71 high +5 mean -235 low
Modmor II	+90	+4 high -120 mean -190 low	+7 high -41 mean -90 low
T-300	+160	+4 high -118 mean -242 low	+5 high -81 mean -146 low
Magnamite II	+160	+80 high +17 mean -45 low	-85 high -99 mean -114 low
Pure Graphite	+120	+120 high +55 mean -73 low	+96 high +20 mean -54 low

Table VI. Open Circuit Corrosion Potential (ϕ_{corr}) after 24 Hrs in 3.5% NaCl Solution, Corrosion Potentials Before (ϕ_{corr}), and After (ϕ^{e}_{corr}) Galvanic Couple Test for Graphite Materials, 3.5% NaCl Solution, pH-7, 22$\pm$ 1^{o}C

ϕ_{corr} values in the first data column were determined in a 24 hour open-circuit corrosion potential test using the method illustrated in Fig. 16. It is realized that even after this extensive period of time, the GECM samples may not have reached an equilibrium potential. Brown and Coomber ran 5 day corrosion potential tests on certain GEC materials and found equilibrium ϕ_{corr} values as high as +300 mv (Ref 12:233). However, this researcher found that the ϕ_{corr} of test GECM samples were increasing almost imperceptibly after 24 hours and are assumed to be near

equilibrium. Notice that these GECM ϕ_{corr} values are very noble. The samples ϕ_{corr} compare in magnitude, and in most cases exceed the ϕ_{corr} determined for pure graphite. The ϕ^{s}_{corr} and ϕ^{e}_{corr} values of the GECM samples were taken after a fifteen minute pre-test and post-test

No.	Coupled To	$\bar{i}_{gcd}$ ($\mu A/cm^2$)	r_g (mdd)	r_g (mpy)	r_A (mpy)	$\Delta\phi^{s}_{corr}$ (mv)	Overall No.
1	2020 T651	17.9	18.6	9.72	13.5	-654	2
2	7075 T6	12.5	12.6	6.5	24.2	-771	5
3	MA-87(73)	10.4	10.7	5.7	30.6	-935	6
4	2024 T6	10.3	10.6	5.6	20.1	-621	8
5	2024 T3	8.7	9.0	4.8	31.2	-703	10
6	MA-87(72)	7.1	7.2	3.9	30.6	-845	12
7	Al-Gr	5.2	4.8	2.8	69.9*	-805	13

*Severe crevice corrosion

Table VII. Galvanic Series for GECM Coupled with Aluminum Alloys in 3.5% NaCl Solution

delay. An average ϕ^{s}_{corr} and ϕ^{e}_{corr} are shown for the materials with the corresponding high and low values. The wide variations in the ϕ^{s}_{corr} values were due to the fact that the GECM did not have sufficient time to equilibrate (24 hours required). Values of ϕ^{e}_{corr} likewise varied, and was in fact further influenced by effects of the prior galvanic coupling.

Galvanic Current Data Galvanic current i_g versus time plots are shown in Figs. 21 to 41 in the Appendices. Values of average galvanic current $\bar{i}_g$ determined from graphical integration of the time versus i_g plots

were then divided by the galvanic reaction surface, which was approximately 17 cm^2 for most samples, to give the average galvanic current density $\bar{i}_{gcd}$. This value along with the galvanic corrosion rates r_g in both mdd and mpy are listed in Tables VII through XI. Each of these tables ranks the alloy within its alloy type according to its galvanic corrosion susceptibility. Also listed is the couples overall galvanic

No.	Coupled To	$\bar{i}_{gcd}$ ($\mu A/cm^2$)	r_g (mdd)	r_g (mpy)	r_A (mpy)	$\Delta\phi^s_{corr}$ (mv)	Overall No.
1	4340	21.7	53.7	9.9	45.5	-608	1
2	300M	17.2	42.7	7.9	5.9	-249	3
3	*10 Ni Mod	15.7	38.7	7.1	5.2	-517	4
4	4130	10.4	25.9	4.8	75.1	-523	7
5	1020	9.9	24.7	4.1	53.8	-529	9

*Severe pitting occurred on specimen surface.

Table VIII: Galvanic Series for GECM Coupled with Steels in 3.5% NaCl Solution

series ranking. Actual weight loss r_A data is listed for comparison purposes to relate r_g with overall corrosion. The corrosion potential difference at the start of the test $\Delta\phi^s_{corr}$ is shown as a basis of comparing galvanic current results with corrosion potentials. The following paragraphs treat in detail the alloy types, by describing the time dependent galvanic current curves from the Appendices, and the data tables for the alloy type in this section. Table XII is the overall galvanic series which ranks the alloys according to galvanic current density with those possessing high $\bar{i}_{gcd}$ listed first, along with actual

weight-loss data r_A.

Time versus i_g plots for aluminum alloys are shown in Figs. 21 through 25 in Appendix A, while Table VII lists electrochemical and weight-loss data for these alloys. General observations of the aluminum alloy time vs i_g plots indicate that all the alloys except aluminum-graphite (Al-Gr) have an initial i_g in the 150 to 300 μA range. Al-7075-T6 and Al-2020-T651 reach a steady value and hold fairly constant for the test period at a higher rate (200-300 μA) than the other Al alloys. Al-2024 (both T3 and T6) and the powder metallurgy (P/M) alloy MA-87 (both in the 72 and 73forging treatments) initially have a high i_g, that rapidly decreases and stabilizes at a lower rate (150 μA). Aluminum graphite (an advanced composite material) shows a surprisingly low galvanic current (50 μA). The average trends are reflected in Table VII. In general, the aluminum alloys had high $\bar{i}_{gcd}$ and a correspondingly high r_A and $\Delta\phi^s_{corr}$. The r_A of 2020-T651, an experimental alloy containing lithium and cadmium, was low, whereas $\bar{i}_{gcd}$ was high. Al-Gr exhibited atypical behavior by having a very low $\bar{i}_{gcd}$ and an extremely high r_A.

Appendix B (Figs. 26 to 30) shows the time vs i_g plots for steels, while Table VIII lists pertinent electrochemical and weight-loss data for the steels tested. All the steels showed very stable behavior with i_g ranging mostly in the 200 to 300 μA range. The low alloy steels (1020,4130) tend to have lower i_g than the high alloy steels. Also, their i_g seems to decrease with time, whereas for high alloy steels (4340,300M, and 10 Ni Mod), i_g increases. Table VIII shows an interesting trend. It is observed that the high alloy steels have a higher $\bar{i}_{gcd}$ than the low alloy steels, while actual weight-loss data indicates r_A for low alloy steels is much greater than 300M, or 10 Ni Mod. It is

observed that severe pitting occurred on 10 Ni Mod. In general, the steel alloys had very high $\bar{i}_{gcd}$ of about the same magnitude or higher than Al alloys. Note that $\Delta\phi^{s}_{corr}$ for steels is somewhat lower than that of Al alloys, which indicates that their galvanic corrosion susceptibility should be lower if potential alone was considered.

The time vs i_g plots for stainless steels (Appendix C, Figs. 31-35) indicates both the low magnitude of i_g, and the unpredictable or unstable changes in i_g with time. One stainless steel, SS-440C (Fig. 31) experienced moderately high i_g. Table IX shows this rather high $\bar{i}_{gcd}$

No.	Coupled	$\bar{i}_{gcd}$ ($\mu A/cm^2$)	r_g (mdd)	r_g (mpy)	r_A (mpy)	$\Delta\phi^{s}_{corr}$ (mv)	Overall No.
1	SS-440C*	8.18	19.0	3.54	19.87	-298	11
2	SS-301	2.24	5.34	0.98	1.16	-200	14
3	SS-304	1.40	3.26	0.59	nil	-240	16
4	PH 17-7	1.05	2.36	0.44	nil	-233	17
5	AFC 77	1.03	2.32	0.41	nil	-309	18

*Severe pitting occurred on specimen surface.

Table IX. Galvanic Series for GECM Coupled with Stainless Steels in 3.5% NaCl Solution

and the correspondingly high r_A. SS-440C experienced severe pitting. Table IX indicates that the other stainless steels had low $\bar{i}_{gcd}$ and also low r_A. Except for SS-440C, the lower $\Delta\phi^{s}_{corr}$ indicates that stainless steels are more compatible with GECM, as was indicated by $\bar{i}_{gcd}$ data.

Nickel-base or superalloy couple curves are shown in Figs. 36 to

38 of Appendix D, while corrosion data is listed in Table X. The time vs i_g indicate a rapid decrease in i_g to an almost zero value that remained constant throughout the test period. The $\bar{i}_{gcd}$ values are small, and r_A was negligible. Notice the contrast between the low $\bar{i}_{gcd}$ and the relatively large value of $\Delta\phi^{s}_{corr}$ for nickel alloys. This high potential difference would indicate a higher galvanic corrosion, which proves not to be the case.

Titanium alloys, shown in Figs. 39 and 40 in Appendix E, indicate behavior similar to that of the nickel-base alloys, with an even smaller i_g. Table XI indicates the excellent galvanic corrosion resistance of titanium alloys. Here, again $\Delta\phi^{s}_{corr}$ would indicate a much higher galvanic corrosion susceptibility if corrosion potentials

No.	Coupled	$\bar{i}_{gcd}$ ($\mu A/cm^2$)	r_g (mdd)	r_g (mpy)	r_A (mpy)	$\Delta\phi^{s}_{corr}$ (mv)	Overall No.
1	Inconel	0.435	1.15	0.180	nil	-402	19
2	Inconel X	0.055	0.13	0.023	nil	-255	20
3	Rene 41	0.037	0.08	0.014	nil	-428	21

Table X. Galvanic Series for GECM Coupled with Nickel-Base Alloys in 3.5% NaCl Solution

along were considered.

Beryllium-copper (Be-Cu) shown in Fig. 41 of Appendix F was very stable in i_g over the test period. Its $\bar{i}_{gcd}$ (Table XI) was in the range of the stainless steels, and it experienced a small r_A. Its $\Delta\phi^{s}_{corr}$ correlated closely with its low $\bar{i}_{gcd}$.

As a final observation, no great variations in data magnitudes

were obtained from varying the GECM. Data using different GEC materials seemed to fit in well with overall data. No specific GECM caused a decrease or increase in galvanic current in every case.

No.	Coupled	i_{gcd} ($\mu A/cm^2$)	r_g (mdd)	r_g (mpy)	r_A (mpy)	$\Delta\phi_{corr}^{s}$ (mv)	Overall No.
1	Ti 6Al-2Sn 4Zr-2Mo	nil	nil	nil	0.84	-408	22
2	Ti 6Al-4V	nil	nil	nil	6.00	-280	23
-	Be-Cu	1.42	8.06	1.3	1.82	-292	15

Table XI. Galvanic Series for GECM Coupled with Titanium Alloys and Be-Cu in 3.5% NaCl Solution

Discussion

Alloy Behavior From the results obtained above, some explanations for the observed behavior of the alloy/GECM couples can be made. The following discussion is in relation to the behavior of Al alloys. Mansfeld and coworkers observed that Al-7075 uncoupled has a lower corrosion rate in 3.5% NaCl than uncoupled Al-2024 (r_o of 0.95 vs 5.24 mdd respectively) (Ref 20:350). When the two were coupled with a more noble alloy, the Al-7075 alloy had a higher i_g than Al-2024. This is supported by the results of this research. A possible explanation for the high i_g of Al-2020 T651 is the lithium and cadmium alloying elements which are active electrochemically. The P/M MA-87 alloy samples may have experienced reduced i_g due to corrosion product buildup

Overall Ranking	Coupled To	$\bar{i}_{gcd}$ ($\mu A/cm^2$)	r_A (mpy)	Overall Ranking	Coupled To	$\bar{i}_{gcd}$ ($\mu A/cm^2$)	r_A (mpy)
1	4340	21.7	45.5	13	Al-Gr	5.20	69.9
2	2020 T651	17.9	13.5	14	SS-301	2.24	1.16
3	300M	17.2	5.9	15	Be-Cu	1.42	1.82
4	10 Ni-Mod	15.7	5.2	16	SS-304	1.40	nil
5	7075 T6	12.5	24.2	17	PH 17-7	1.05	nil
6	MA-87(73)	10.4	30.6	18	AFC-77	1.03	nil
7	4130	10.4	75.1	19	Inconel	0.435	nil
8	2024 T6	10.3	20.1	20	Inconel X	0.055	nil
9	1020	9.9	53.8	21	Rene 41	0.037	nil
10	2024 T3	8.7	31.2	22	Ti 6Al-2Sn-4Zr-2Mo	0.001	1.82
11	SS-440C	8.2	19.9	23	Ti 6Al-4V	0.000	nil
12	MA-87(72)	7.1	30.6				

Table XII. Galvanic Series For CECM Based on Average Current Density $\bar{i}_{gcd}$ in 3.5% NaCl Solution

on the sample surface which reduced current flow. The reduced $\bar{i}_g$ of the P/M MA-87 (73) over MA-87 (72) could be due to the larger particle sizes of the MA-87 (72) macrostructure which increased the overall area for galvanic reaction to occur (Ref 21:Fig. 11). The high r_A and small $\bar{i}_{gcd}$ for Al-Cr can be explained by the crevice corrosion taking place on the materials surface being so intense locally that the coupling with GECM causes only a small i_g to flow. High corrosion product build-up on the Al-Gr surface could be an added factor in the low $\bar{i}_{gcd}$ measured.

In relation to the observed behavior of steel, La Que found that steels corrode uniformly in seawater, independent of alloying elements up to a point (Ref 22:495). This investigation shows that the r_A of plain carbon 1020 steel and 4130 low-alloy steel were of similar magnitude and that the surface corrosion was largely uniform. Steels 300M and 10Ni Mod had lower r_A due to residual alloy content (Ref 23:21). Their surfaces, however, had localized corrosion product buildup. The lower $\bar{i}_{gcd}$ of 1020 and 4130 and their decreasing i_g with time could be due to the subsequent corrosion product building up uniformly on the alloy surface. Since the higher alloy steels did not have this uniform buildup, i_g did not decrease with time. In fact, there was an increase in i_g with time for 4340, 300M, and 10 Ni Mod steels. An explanation for this increase is that as concentration cell (crevice, pitting) corrosion increases on the surface, the cathodic area is reduced, and more i_g flows to compensate for larger anodic reaction area. Low-alloy steel 4340 displayed both high r_A and $\bar{i}_{gcd}$. Large areas of crevice corrosion were present on the surface accounting for the high r_A. Increasing i_g with time and high i_{gcd} could be due to the decreasing

cathode to anode ratio on the alloy surface.

The unstable nature of the stainless-steels is due to the forming, breaking down, and reforming of passive films. Even with this active-to-passive instability, overall galvanic current was not high. It must be cautioned that stainless steels undergo other forms of corrosion (e.g., pitting) that may make it unacceptable for certain applications. SS-440C displayed a high corrosion rate because it has a low nickel content.

Both nickel base and titanium alloys have excellent corrosion behavior in neutral NaCl solutions because of the natural protective oxide films that form on the alloy surfaces. This film is responsible for the low $\bar{i}_{gcd}$ in 3.5% NaCl. Rozenfel'd and coworkers discuss titanium when it acts as an anode (Ref 24:634). The TiO_2 (rutile) film forms an electrical barrier which greatly reduces current.

The Be-Cu alloy contained mostly copper. Its low corrosion rate was due to the nobility of copper. In this case, use of potential difference would have indicated the small galvanic corrosion.

Potential vs Galvanic Current for Galvanic Corrosion Estimates. A comparison of the galvanic series based upon potential considerations in Table V, and that based upon galvanic current density in Table XII dramatically illustrates the problems that may be encountered when potential difference is used to predict galvanic corrosion. The ideal galvanic corrosion properties of titanium and nickel base alloys would be overlooked if potential difference were the criteria. Galvanic corrosion reactions are determined by the oxidation and reduction reaction kinetics. The galvanic series listed in Table XII is a more reliable indicator of corrosion acceleration due to galvanic coupling.

Acceptability Criteria. Table XII lists the alloys according to the magnitude of the average galvanic current density, and can be successfully used by a designer only if the increase of corrosion rate due to galvanic coupling is the primary corrosion mode. The alloy considered may be unacceptable due to the existence of one or more of the other forms of corrosion. Like Mansfeld, this researcher arbitrarily classifies the alloys tested into three groups. Group I couples are those that exhibited $\bar{i}_{gcd}$ less than 5 μA and are considered acceptable. Group II couples are considered borderline and have $\bar{i}_{gcd}$ values between 5 and 15 μA. Unacceptable couples would be those with average galvanic current densities greater than 15 μA. Table XIII lists the alloys according to this criteria.

Correlation of Average Galvanic Current Density and Galvanic Corrosion Determined from Weight-Loss Tests. Tables VI through XI list the values of r_g for the various alloys. It is noted that there is a large discrepancy between this value and r_A. This is because r_A is a sum of both r_g and the uncoupled corrosion rate of the alloy r_o. Mansfeld states that the best correlation between average galvanic current density $\bar{i}_{gcd}$ and rates determined from weight-loss tests is found through the empirical relation: (Ref 20:349)

$$\bar{i}_{gcd} = k\ (r_A - r_o) \tag{20}$$

where k is the factor that must be found to relate galvanic current measurements to the actual corrosion rate of an alloy in a particular environment. The use of this empirical relationship requires accurate weight-loss data to determine r_A and r_o. Once k is derived, continuous monitoring of galvanic current instead of intermittent weight-loss tests,

GROUP	ALLOY COUPLED TO GECM
I ACCEPTABLE ($\bar{i}_{gcd}$ < 5 μA/cm^2)	Ti-6Al-4V Ti-6Al-2Sn-4Zr-2Mo Rene 41 Inconel X Inconel AFC-77 PH 17-7 SS-304 Be-Cu SS-301
II BORDERLINE (5 μA/cm < $\bar{i}_{gcd}$ < 15 μA/cm^2)	Al-Gr MA-87(72) SS-440C 2024-T3 1020 2024-T6 4130 MA-87(73) 7075-T6
III UNACCEPTABLE ($\bar{i}_{gcd}$ > 15 μA/cm^2)	10 Ni Mod 300M 2020-T651 4340

Table XIII. Acceptability Criteria for Alloys Tested

in a system whose corrosion variables remain constant, would be a considerable aid in corrosion predictions. In this study, r_A data is questionable and very little r_o data was found. However, using r_o data for Al-7075 and Al-2024 given by Mansfeld, and the corresponding r_A data from this study, a k of about 0.5 μA/mpy was determined for these aluminum alloys/GECM couples. This result is very inconclusive because of the limited data. Much more research is required to determine r_o and r_A data for the various alloys/GECM couples to make this a viable method for exact galvanic corrosion measurements.

Actual Galvanic Corrosion. Many factors that occur in actual corrosion environments would make the results of this laboratory study less conclusive. In dealing with atmospheric corrosion, as would be the case with aircraft structures, several factors must be considered. Area effect (cathode-to-anode ratio) mentioned previously would be of major concern. Another important consideration would be the corrosive environment. Distance effect is also present in the atmospheric galvanic corrosion because moisture tends to collect at the dissimilar material joint, and galvanic corrosion intensity is greatest at this point, decreasing with distance away from the joint. Another aspect of corrosion not treated in this study is the use of sealants, inhibitors, and protective coatings. The primary concern of this research has been to establish compatible couples. Use of corrosion preventative measures can make these couples even more corrosion resistant. Researchers have found that many sealants, coatings, and inhibitors aid in controlling galvanic corrosion of GECM/alloy couples (Ref 5:16, Ref 25:5, Ref 16:13). One of the best methods of joining graphite epoxy composite materials to various alloys is to use adhesive bonding (Ref 5:17, Ref 25:11).

In this method, care must be taken that the metal surface is free of abrasions; otherwise, the adhesive layer may be ruptured and galvanic attack accelerated in the presence of moisture.

Conclusions

From the results of this research, the following conclusions are made:

1. Potential difference measurement is a poor indicator of the extent of galvanic corrosion experienced when GECM is coupled with an alloy.
2. Continuous i_g data monitoring gives the time dependent variations in galvanic corrosion rates more readily than conducting weight-loss tests.
3. A galvanic series based upon average galvanic current density was developed in Table XII. Compatibility of alloy types were as follows. Steels and aluminum alloys were least compatible. Stainless steels and Be-Cu were better. The best alloys were nickel-base and titanium.
4. Table XIII classifies the alloys into three arbitrary groups: (1) Acceptable, (2) Borderline, and (3) Unacceptable.
5. Very little difference was found in the corrosion potentials of the various GEC materials.
6. No particular GECM was found superior, or inferior, in reducing galvanic corrosion.

The following recommendations are made:

1. Continue research to refine data by making more tests with the couples tested using a larger variety of GECM materials.

2. Expand the galvanic series by testing other alloys.
3. Conduct galvanic corrosion tests in other media.
4. Conduct galvanic corrosion tests using protective coatings and sealants.
5. Conduct long term tests (5 days or more) to compare with 24 hour test results.

Bibliography

1. Uhlig, H. H. Corrosion and Corrosion Control, New York: John Wiley & Sons, Inc., 1963.

2. Hercules, Incorporated. Graphite Materials, Magma, Utah: Systems Group, Bacchus Works, 1975.

3. Randolph, R. E., et al. Graphite Composite Landing Gear Components-Side Brace Assembly and Torque Link for A-37B Aircraft, AFFDL-TR-73-69, Wright-Patterson Air Force Base, Ohio, Air Force Flight Dynamics Laboratory, May 1973.

4. Dexter, Peter F. Graphite Epoxy Landing Gear Environment Tests, AFFDL-TM-74-217 FEM, Wright-Patterson Air Force Base, Ohio, Air Force Flight Dynamics Laboratory, November 1974.

5. Johnston, G. R., et al. Galvanic Corrosion Effects Associated With Graphite Composite/Metal Joints, Lockheed Report LR-26088, Burbank, California, The Lockheed Company, November 1973, AD-776425

6. Fontana, M. G. and N. D. Greene. Corrosion Engineering, New York: McGraw-Hill Book Co., 1967.

7. Vetter, K. J. Electrochemical Kinetics, New York: Academic Press, 1967.

8. Bockris, J.O.M. and A. K. Reddy. Modern Electrochemistry, Vol. II. New York, Plenum Press, 1970.

9. Uhlig, H. H. The Corrosion Handbook, New York: John Wiley and Sons, Inc., 1948.

10. Mansfeld, F. "Using Electrochemical Techniques," paper presented at the Seminar on the Performance of Condensers in Nuclear and Fossil Power Plants, Columbus, Ohio, The Ohio State University, 2-4 June 1975.

11. Whitman, W. G. and R. P. Russell. "The Natural Water Corrosion of Steel in Contact with Copper," Industrial Engineering Chemistry, Vol. 16, 27C (1957).

12. Brown, A.R.G. and D. E. Coomber. "Behavior of Couples of Aluminum and Plastics Reinforced with Carbon Fibre in Aqueous Salt Solutions," British Corrosion Journal, Vol. 7, 233 (1972).

13. Hoare, J. P. The Electrochemistry of Oxygen, New York, Interscience Publishers, Division of John Wiley and Sons, Inc., 1968.

14. Berl, W. G. "A Reversible Oxygen Electrode," Transactions of the Electrochemical Society, Vol. 83, 253 (1943).

15. Yeager, E., P. Krouse and K. V. Rao. Electrochemical Acta, Vol. 9, 1057 (1964).

16. Fischer, P. and J. J. DeLuccia. "Effects of Graphite-Epoxy Composite Materials on the Corrosion Behavior of Aircraft Alloys," Naval Air Development Center, paper presented at the Tri-Service Corrosion Conference, Wright-Patterson Air Force Base, Ohio, 1974.

17. Von Fraunhofer, J. A. and C. H. Banks. The Potentiostat and Its Applications, London, Butterworths, 1972.

18. Devay, J., B. Lenyel Jr., and L. Meszaros. Acta Chemistry Hungaria, Vol. 62, 157 (1969).

19. American Society for Testing and Materials. 1974 Annual Book of ASTM Standards, Part 10, Philadelphia, Pennsylvania, ASTM, 1974.

20. Mansfeld, F., D. H. Hengstenberg, and J. V. Kenkel. "Galvanic Corrosion of Al Alloys-I, Effect of Dissimilar Metals," Corrosion, Vol. 30, 343 (1974).

21. Otto, W. L. "Metallurgical Factors Controlling Structure in High Strength Aluminum P/M Products," Contract F-33615-74-C-5077, First Semi-Annual Report, Alcoa Center, Pennsylvania, Fabricating Metallurgy Division, Alcoa Laboratories, October 15, 1974.

22. La Que, F. L. "Corrosion Testing," Proceedings of ASTM, Vol. 51, 495 (1951).

23. Fink, F. W. and W. K. Boyd. The Corrosion of Metals in Marine Environments, Defense Metals Information Center (DMIC) Report 245, Columbus, Ohio, Bayer and Company, Inc., 1970.

24. Rozenfel'd, I. L., et al. "Some Peculiarities of the Cathodic Behavior of Titanium in Neutral Media," Protection of Metals, Vol. 8, 634 (1972).

25. Brown, A.R.G. and D. E. Coomber. "The Resistance to Corrosion of Some Insulated Carbon Reinforced Plastic to Aluminum Alloy Joints," RAE TR-72160, Farnsbourough, England, Royal Aircraft Establishment, August 1972.

Appendix A

Galvanic Current vs Time for
GECM - Aluminum Alloy Couples

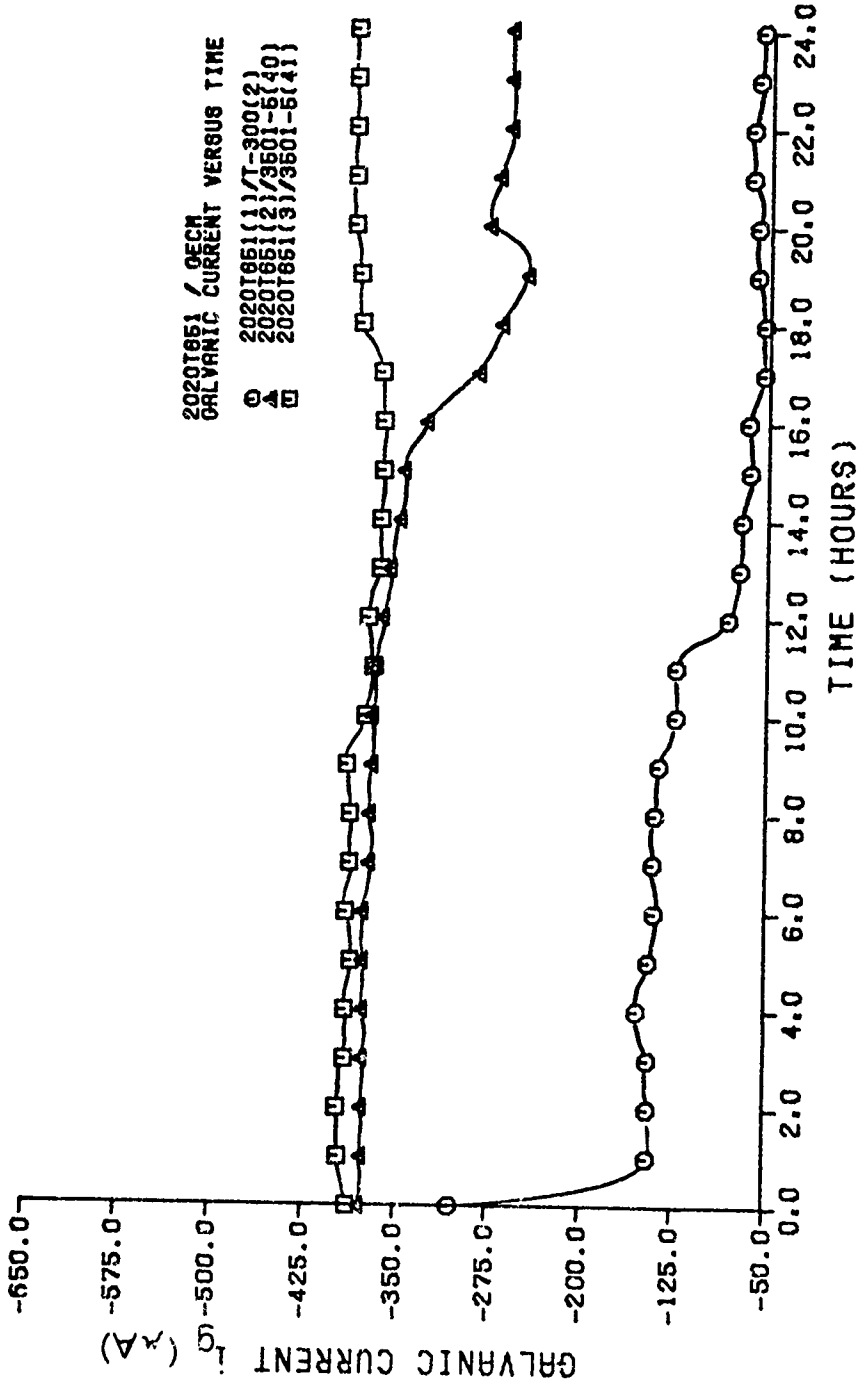

Fig. 21. Galvanic Current vs Time for Al-2020 T651/GECM Couples in 3.5% NaCl Solution at Ambient Temperature

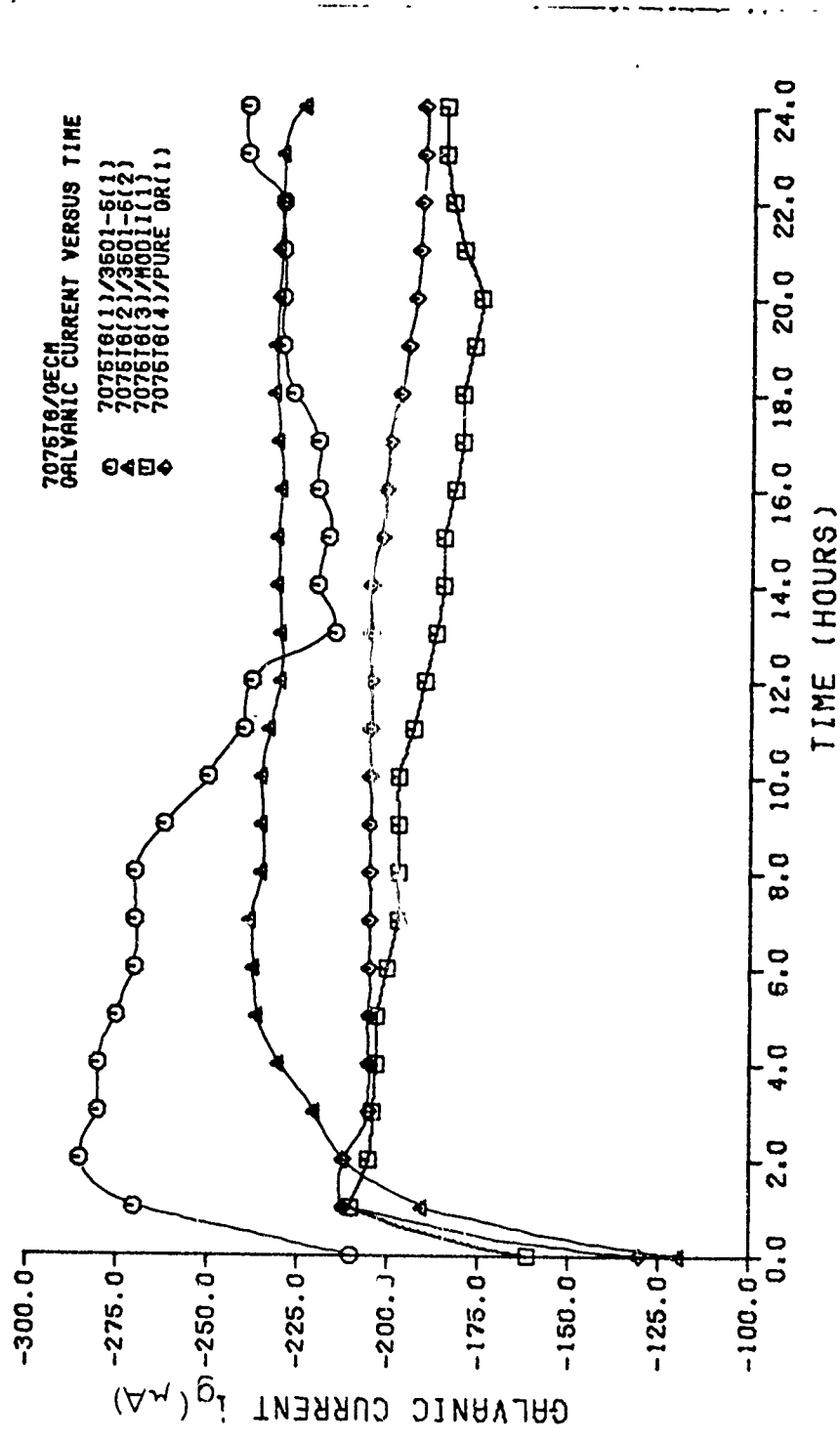

Fig. 22. Galvanic Current vs Time for Al-7075 T6/GECM Couples in 3.5% NaCl Solution at Ambient Temperature

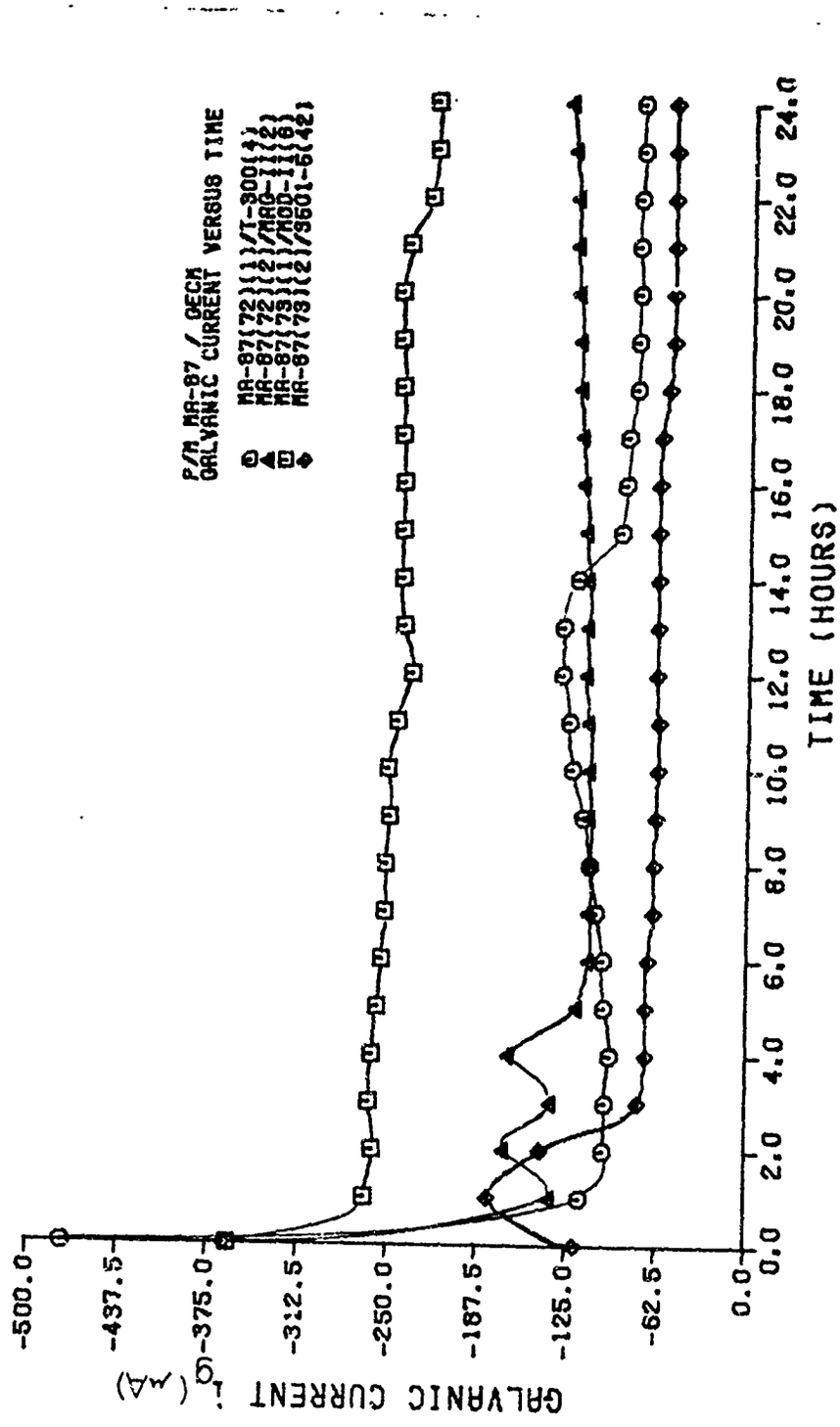

Fig. 23. Galvanic Current vs Time for MA-87 P/M Al Alloy/GECM Couples in 3.5% NaCl Solution at Ambient Temperature

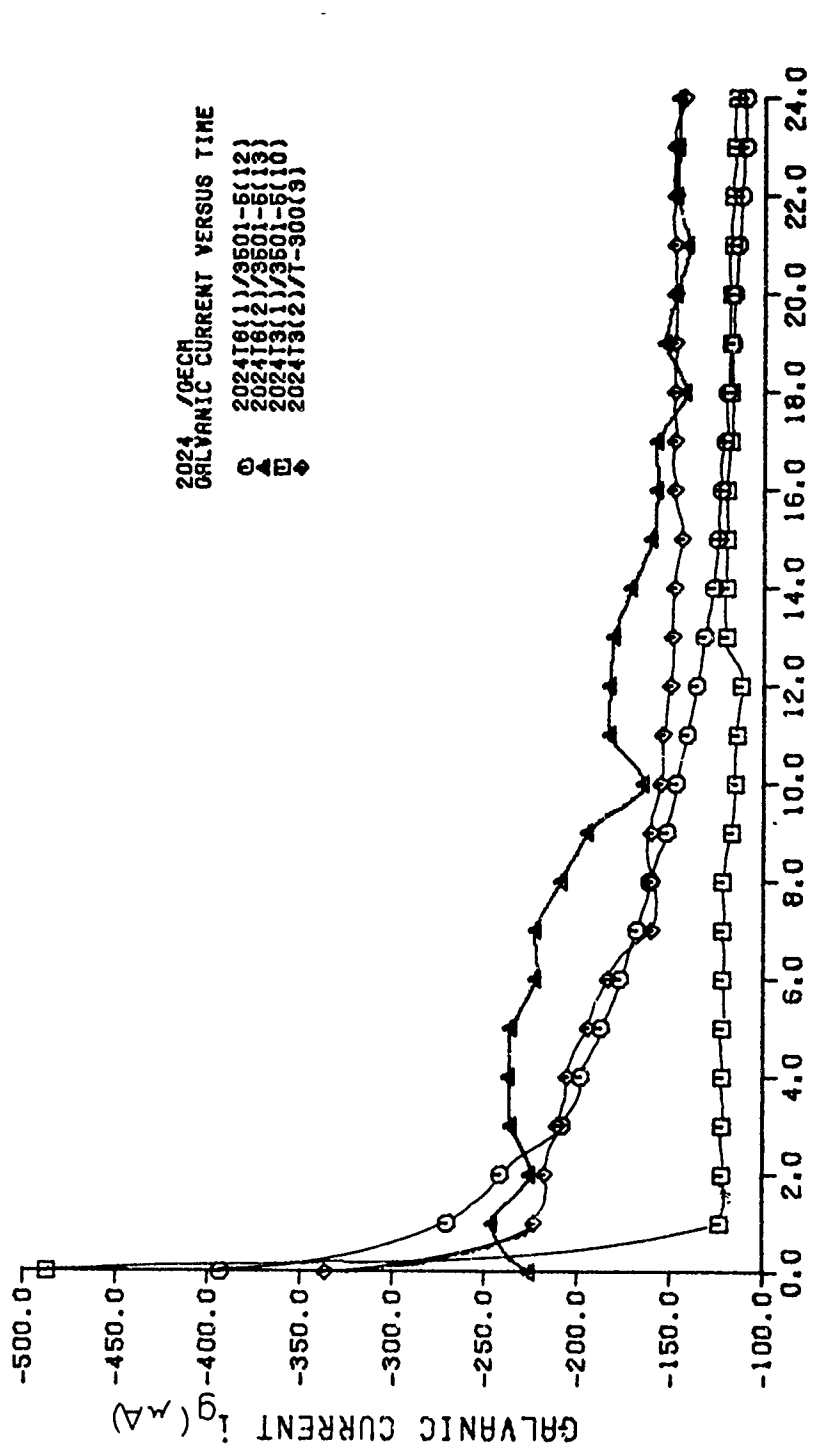

Fig. 24. Galvanic Current vs Time for Al-2024/GECM Couples in 3.5% NaCl Solution at Ambient Temperature

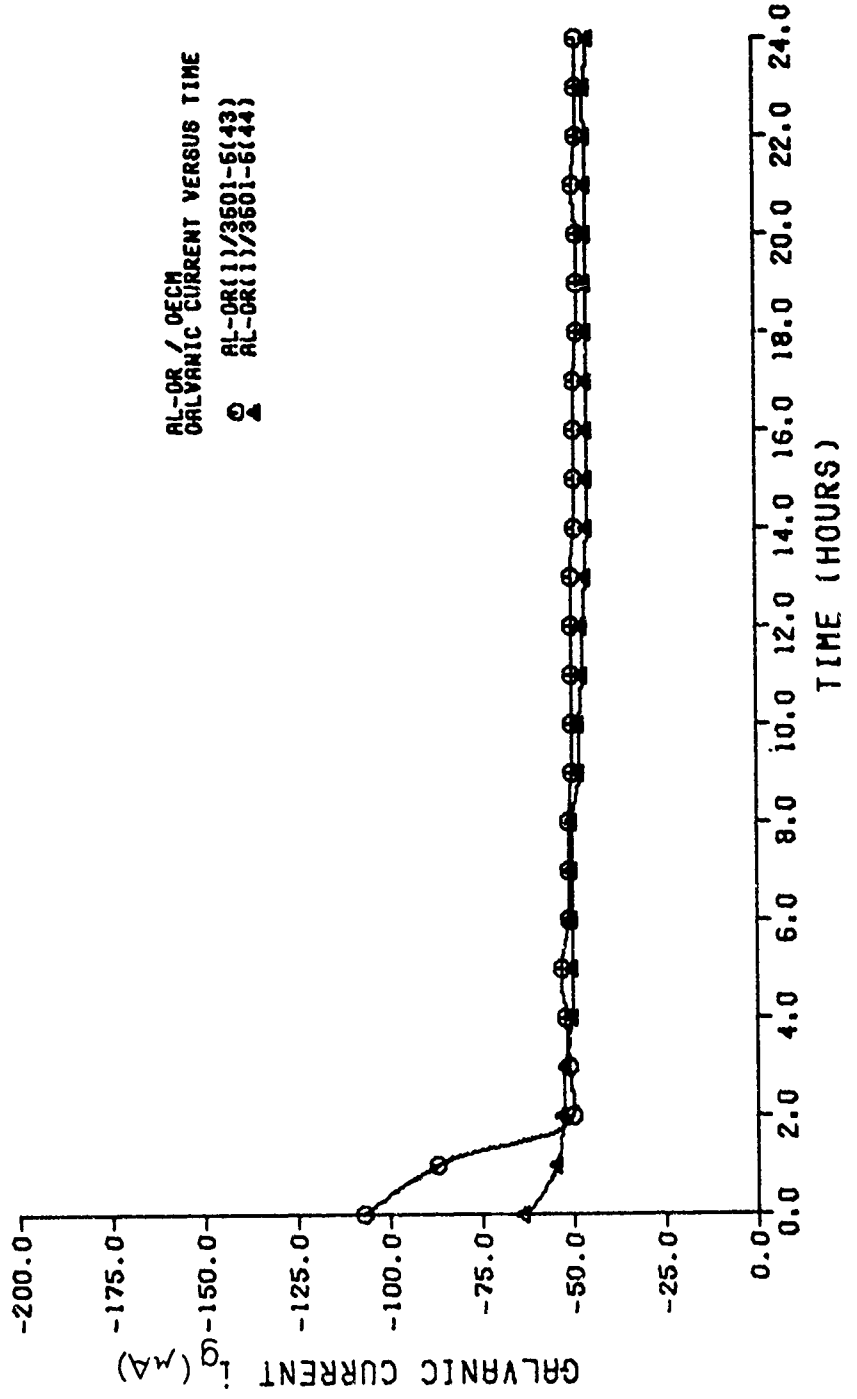

Fig. 25. Galvanic Current vs Time for Al-Gr/GECM Couples in 3.5% NaCl Solution at Ambient Temperature

Appendix B

Galvanic Current vs Time

for GECM - Steel Couples

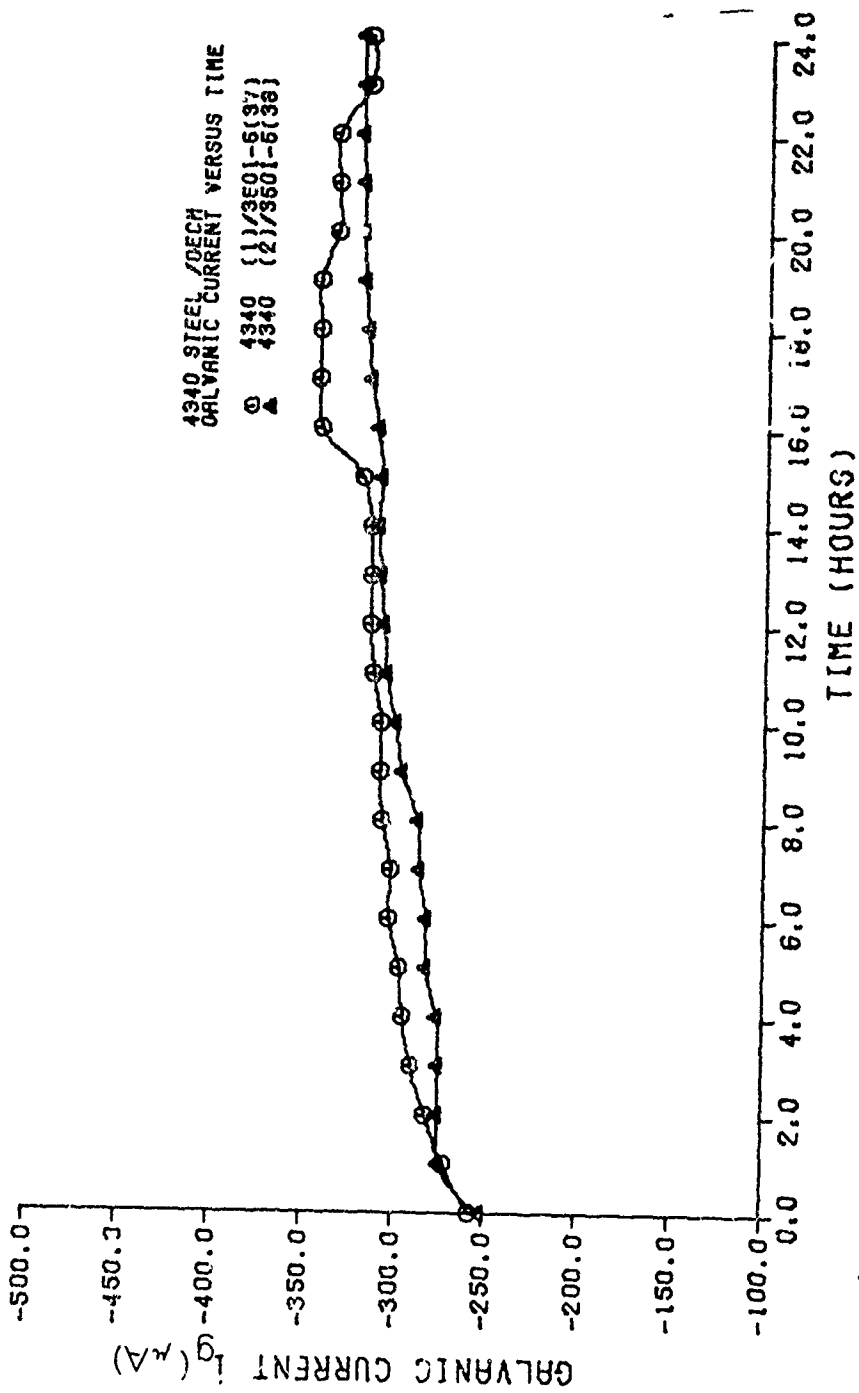

Fig. 26. Galvanic Current vs Time for 4340 Steel/GECM Couples in 3.5% NaCl Solution at Ambient Temperature

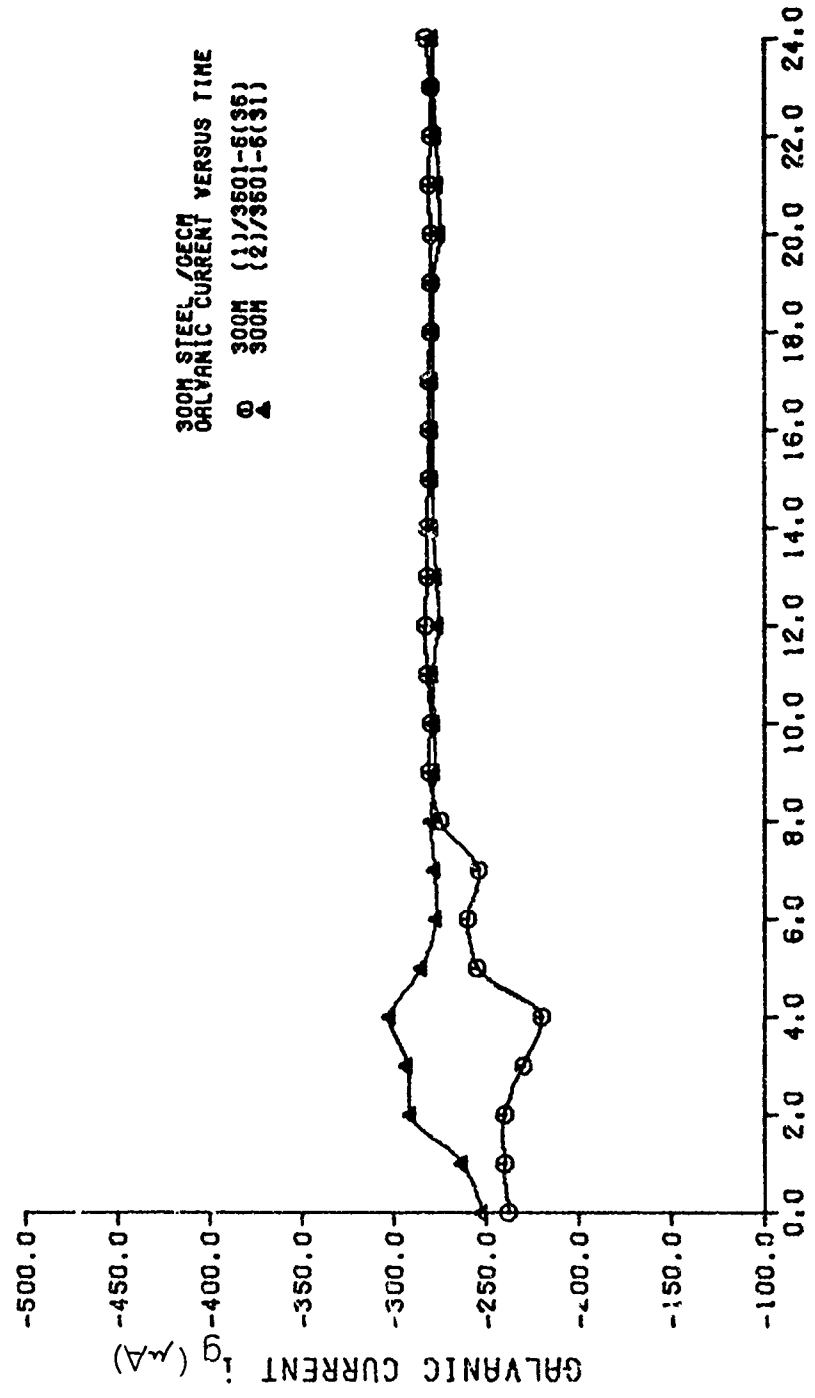

Fig. 27. Galvanic Current vs Time for 300M Steel/GECM Couples in 3.5% NaCl Solution at Ambient Temperature

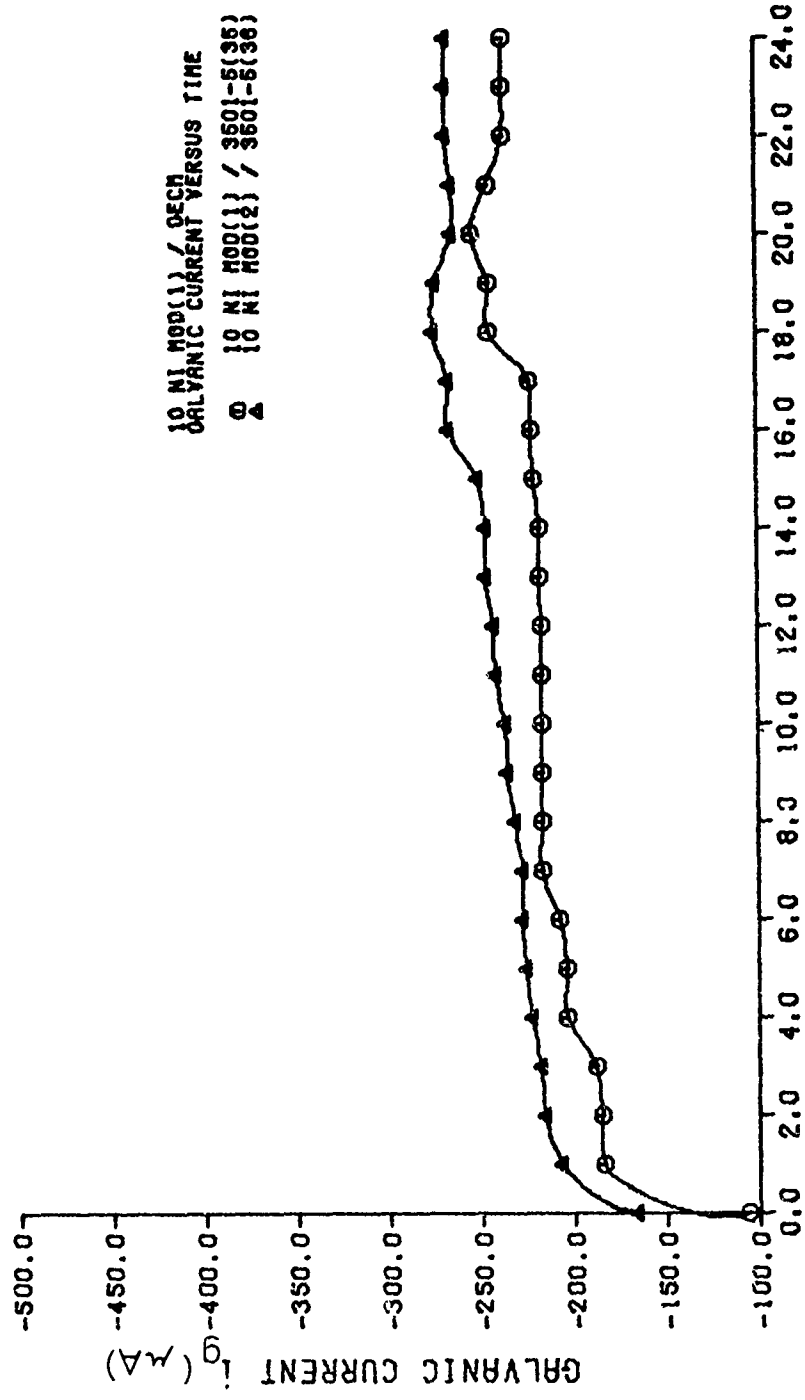

Fig. 28. Galvanic Current vs Time for 10% Ni Mod Steel/GECM Couples in 3.5% NaCl Solution at Ambient Temperature

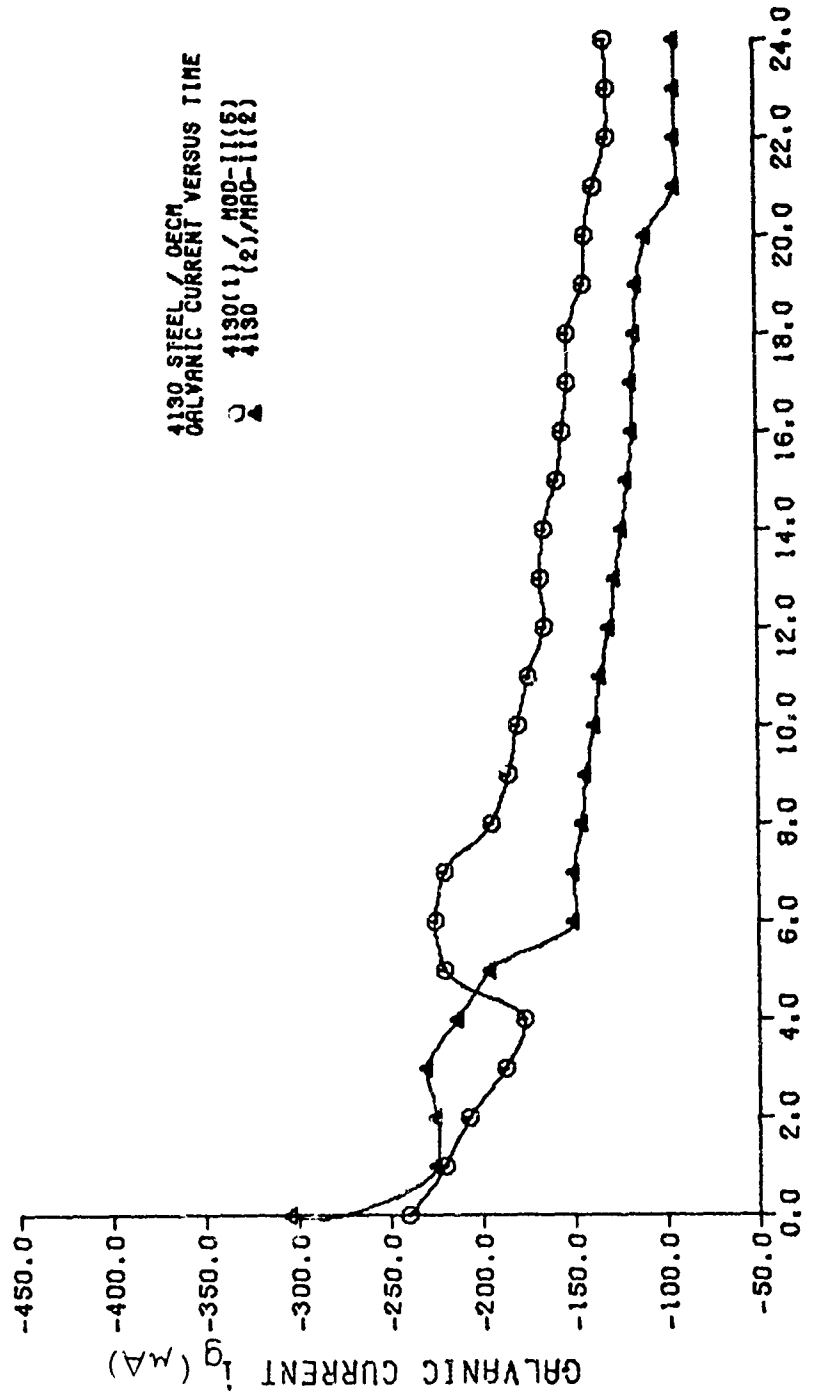

Fig. 29. Galvanic Current vs Time for 4130 Steel/GECM Couples in 3.5% NaCl Solution at Ambient Temperature

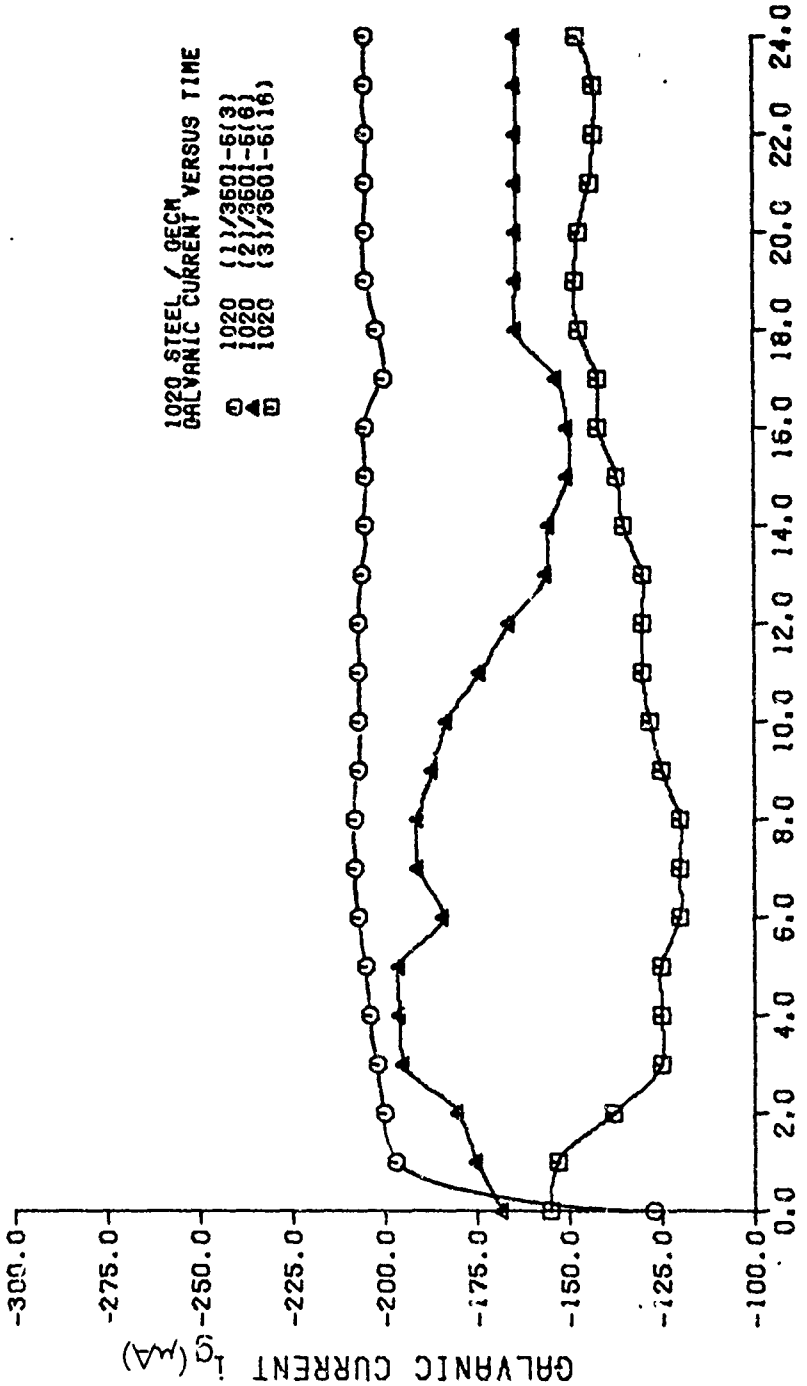

Fig. 30. Galvanic Current vs Time for 1020 Steel/GECM Couples in 3.5% NaCl Solution at Ambient Temperature

Appendix C

Galvanic Current vs Time for

GECM - Stainless Steel Couples

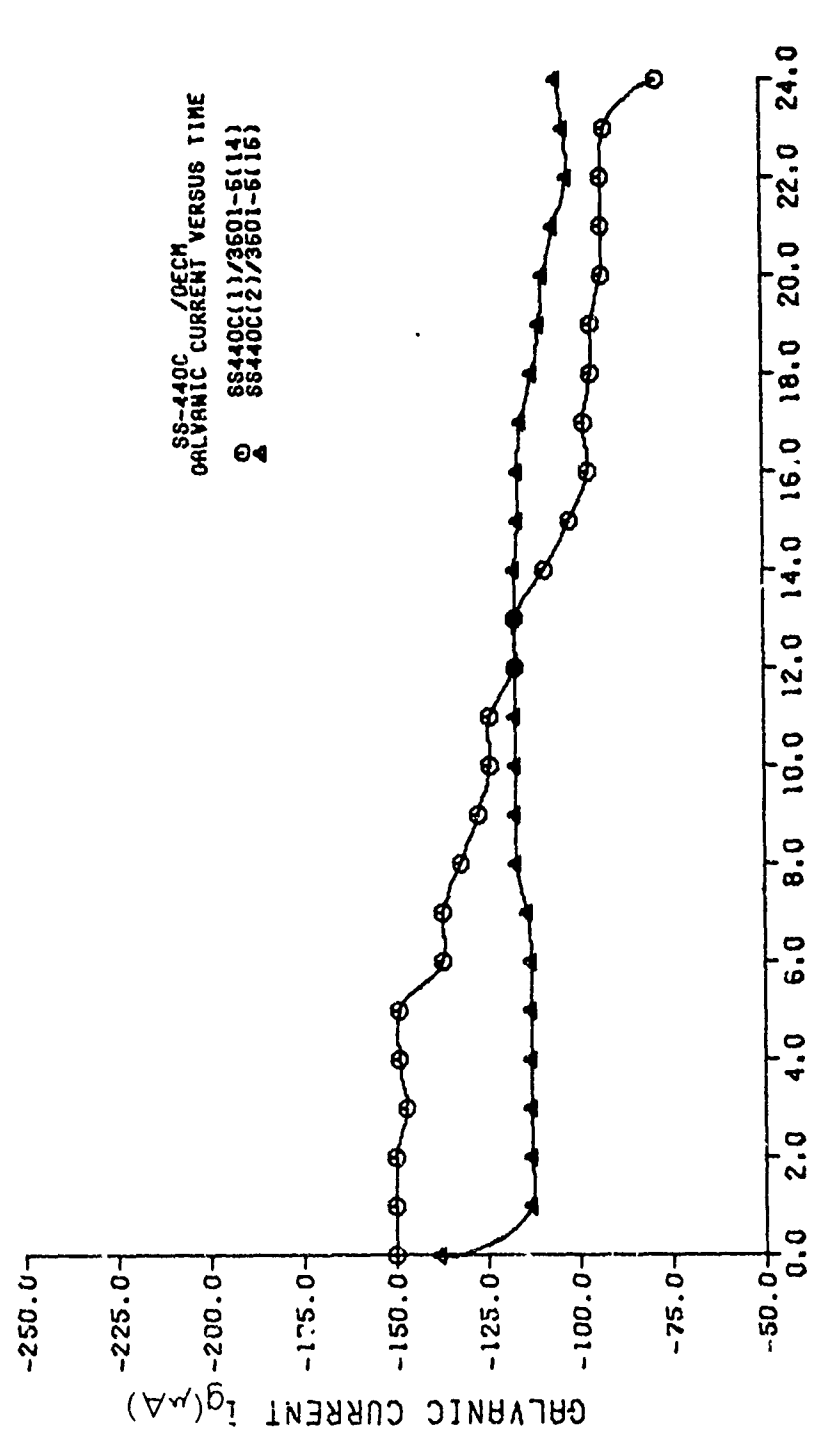

Fig. 31. Galvanic Current vs Time for SS-440C Stainless Steel/GECM Couples in 3.5% NaCl Solution at Ambient Temperature

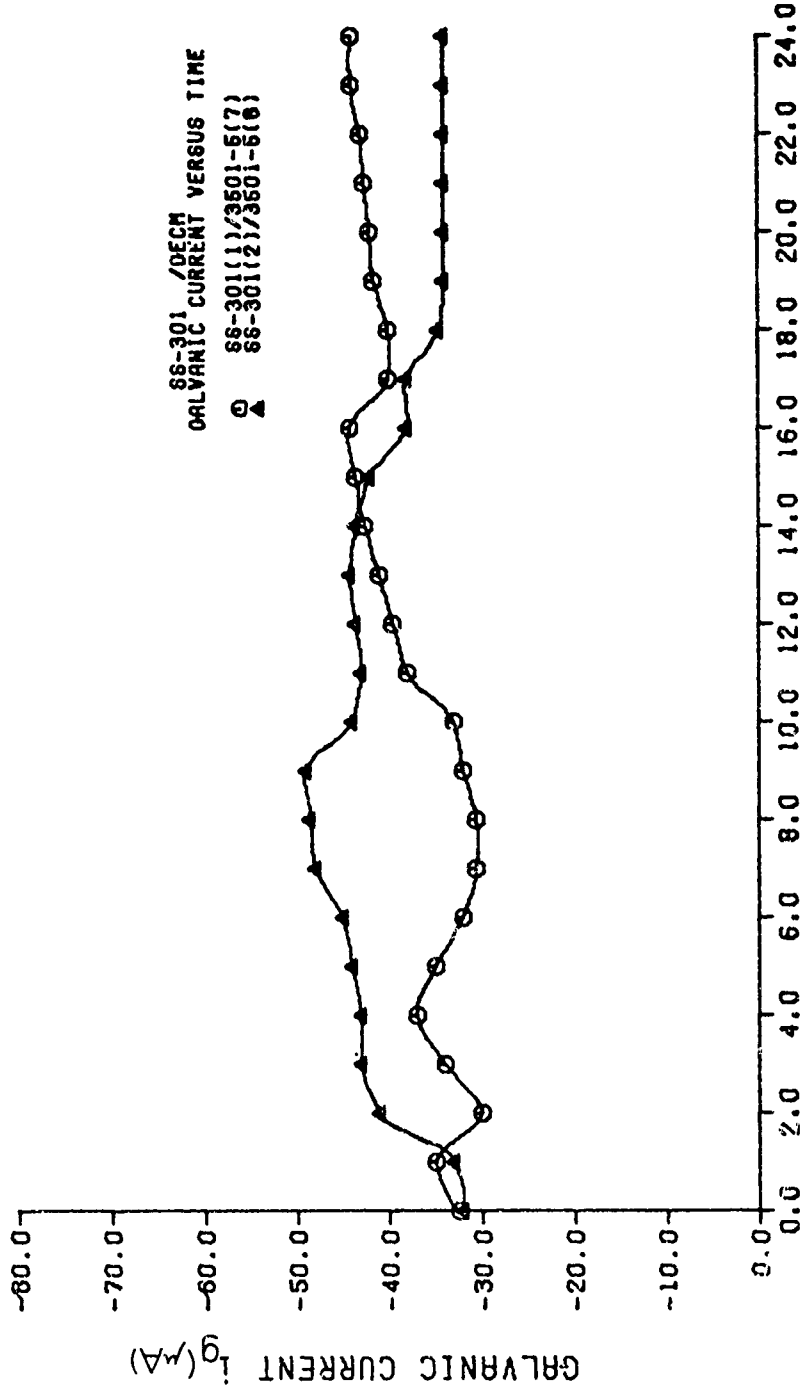

Fig. 32. Galvanic Current vs Time for SS-301 Stainless Steel/GECM Couples in 3.5% NaCl Solution at Ambient Temperature

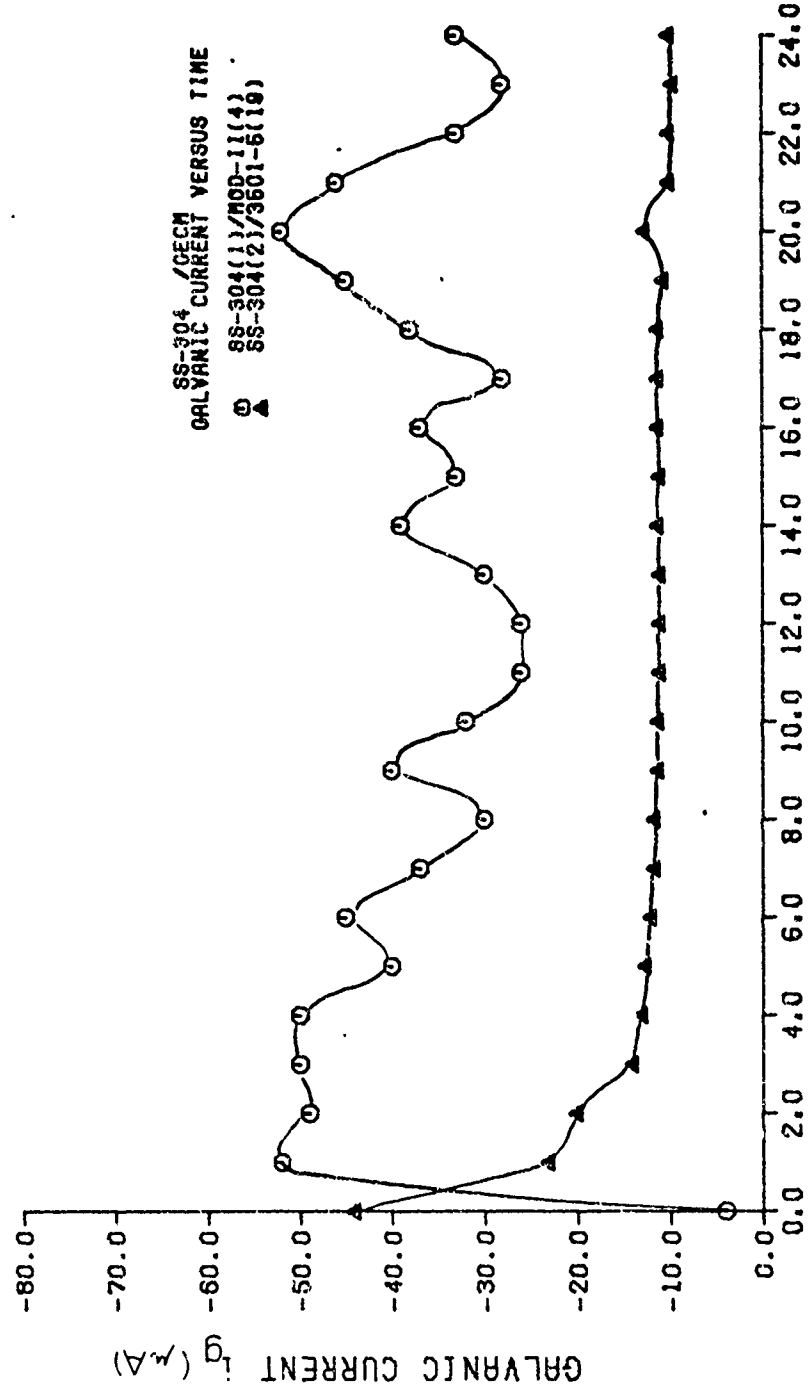

Fig. 33. Galvanic Current vs Time for SS-304 Stainless Steel/GECM Couples in 3.5% NaCl Solution at Ambient Temperature

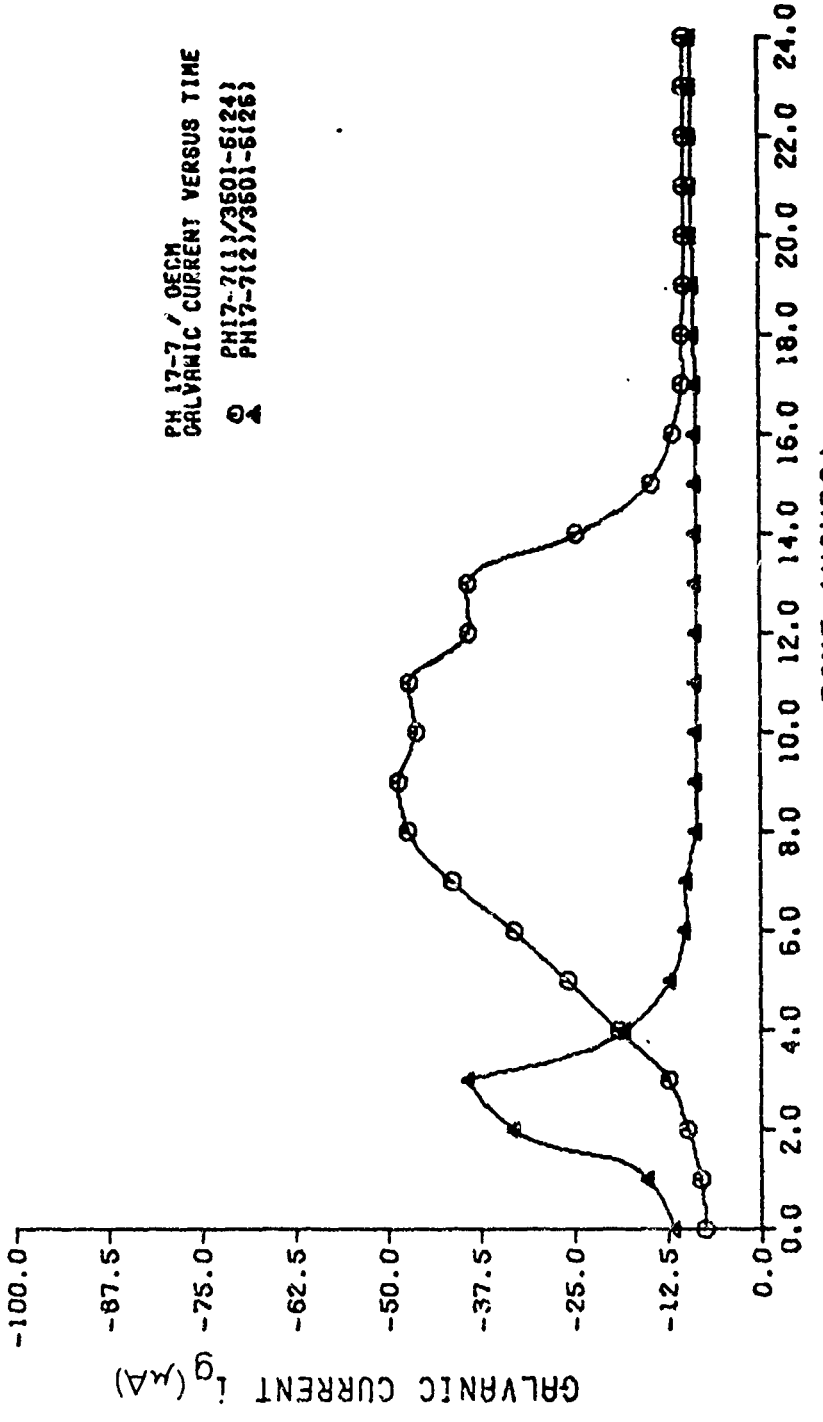

Fig. 34. Galvanic Current vs Time for PH 17-7 Stainless Steel/GECM Couples in 3.5% NaCl Solution at Ambient Temperature

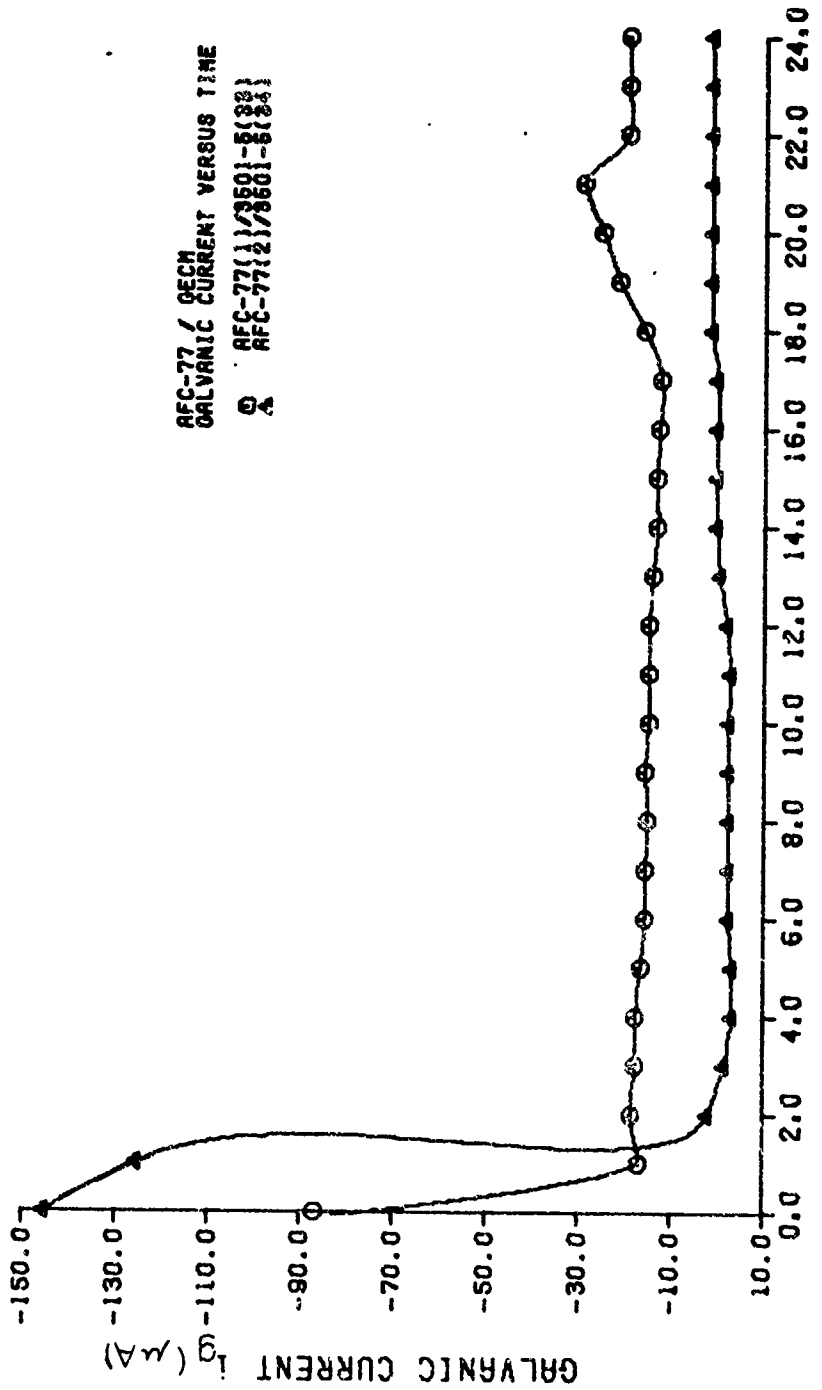

Fig. 35. Galvanic Current vs Time for AFC-77 Stainless Steel/GECM Couples in 3.5% NaCl Solution at Ambient Temperature

Appendix D

Galvanic Current vs Time for
GECM - Nickel Base Alloy Couples

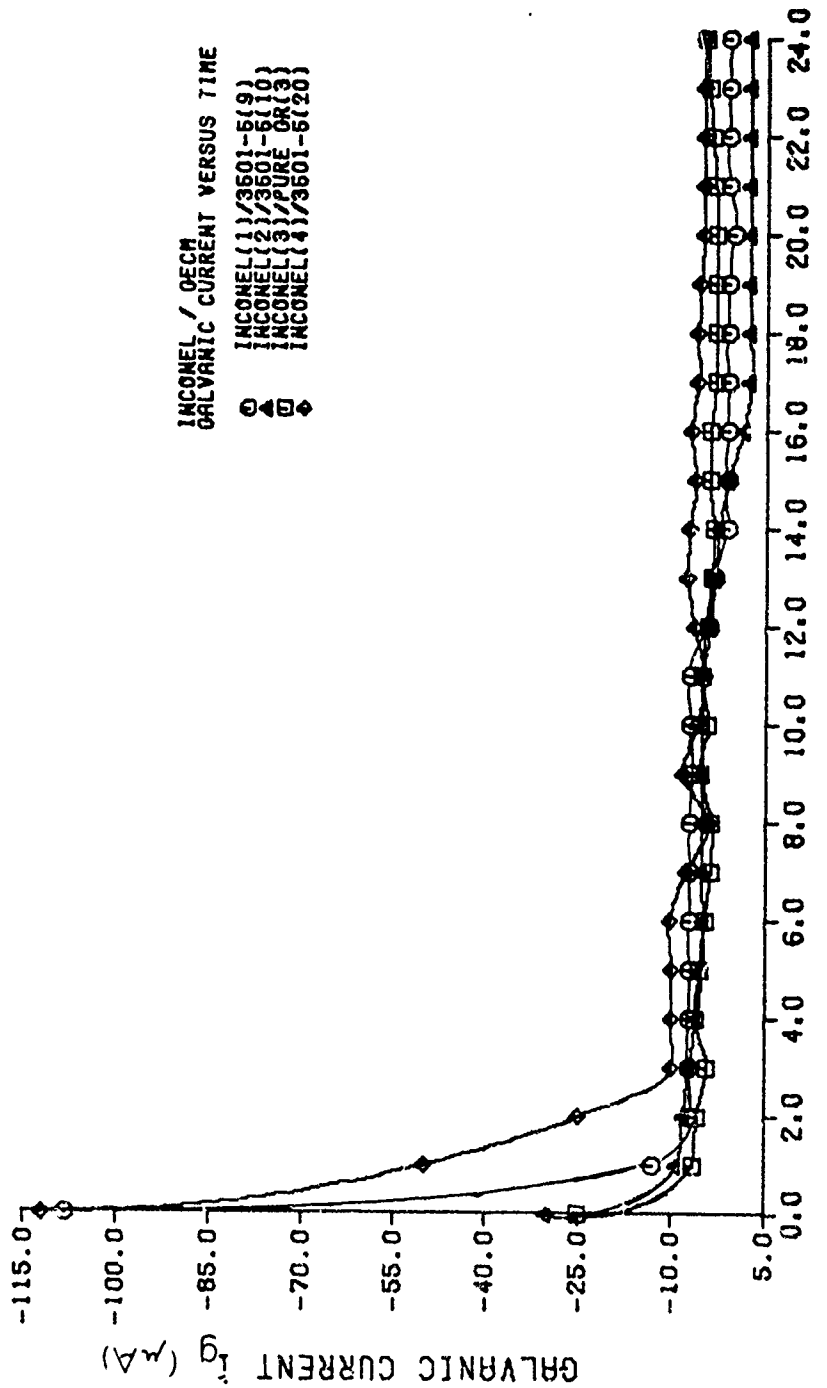

Fig. 36 Galvanic Current vs Time for Inconel/GECM Couples in 3.5% NaCl Solution at Ambient Temperature

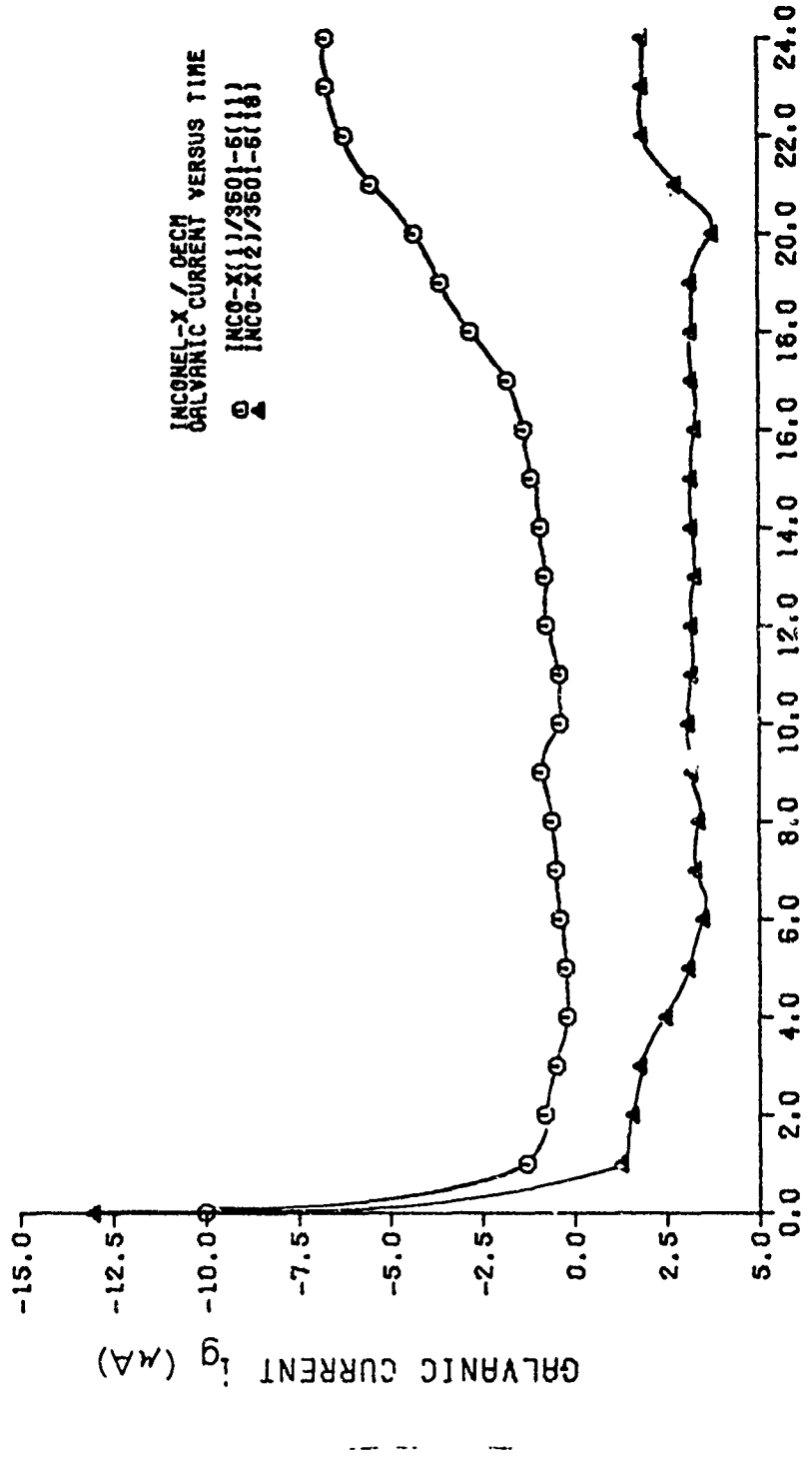

Fig. 37. Galvanic Current vs Time for Inconel X / GECM Couples in 3.5% NaCl Solution at Ambient Temperature

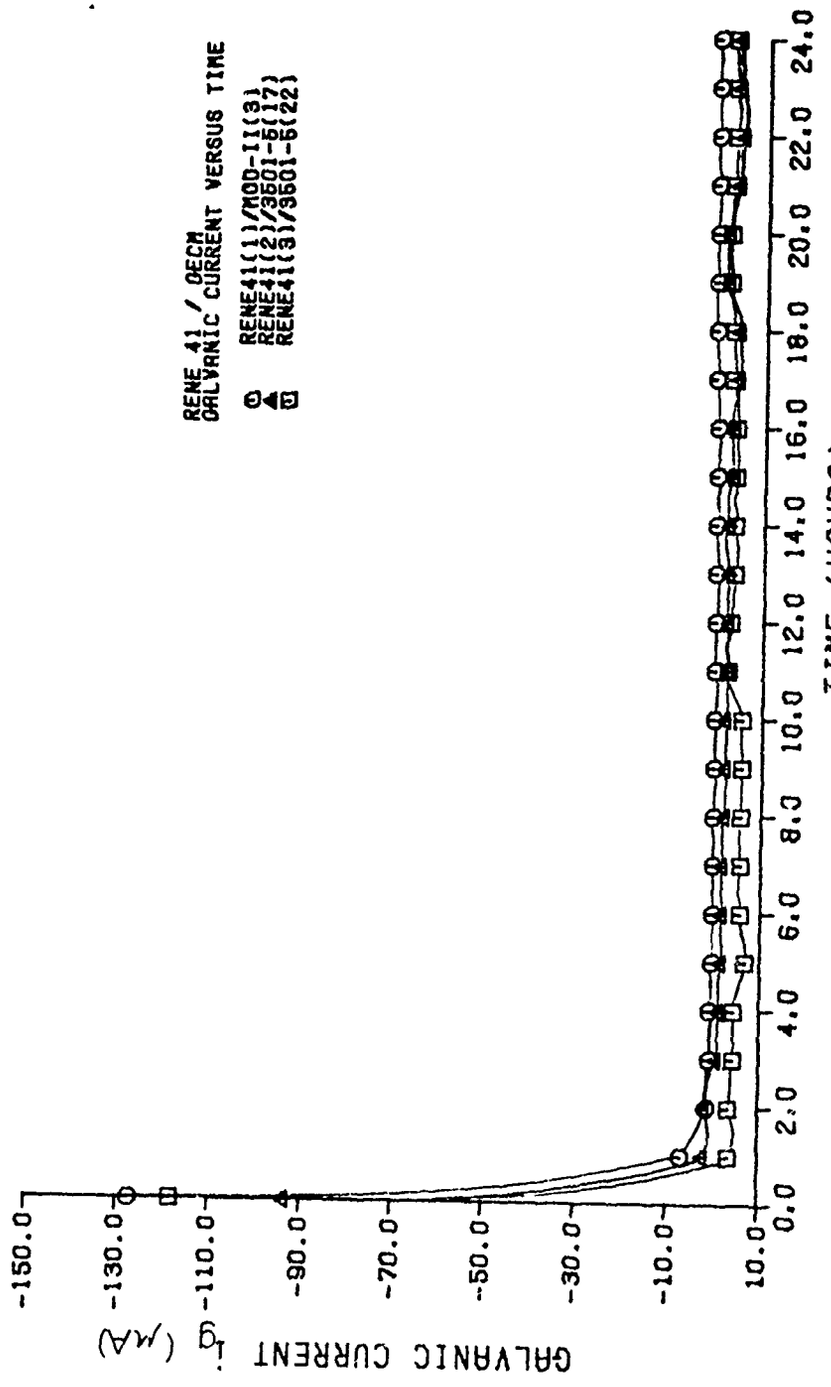

Fig. 38. Galvanic Current vs Time for Rene 41 / GECM Couples in 3.5% NaCl Solution at Ambient Temperature

Appendix E

Galvanic Current vs Time for
GECM - Titanium Alloy Couples

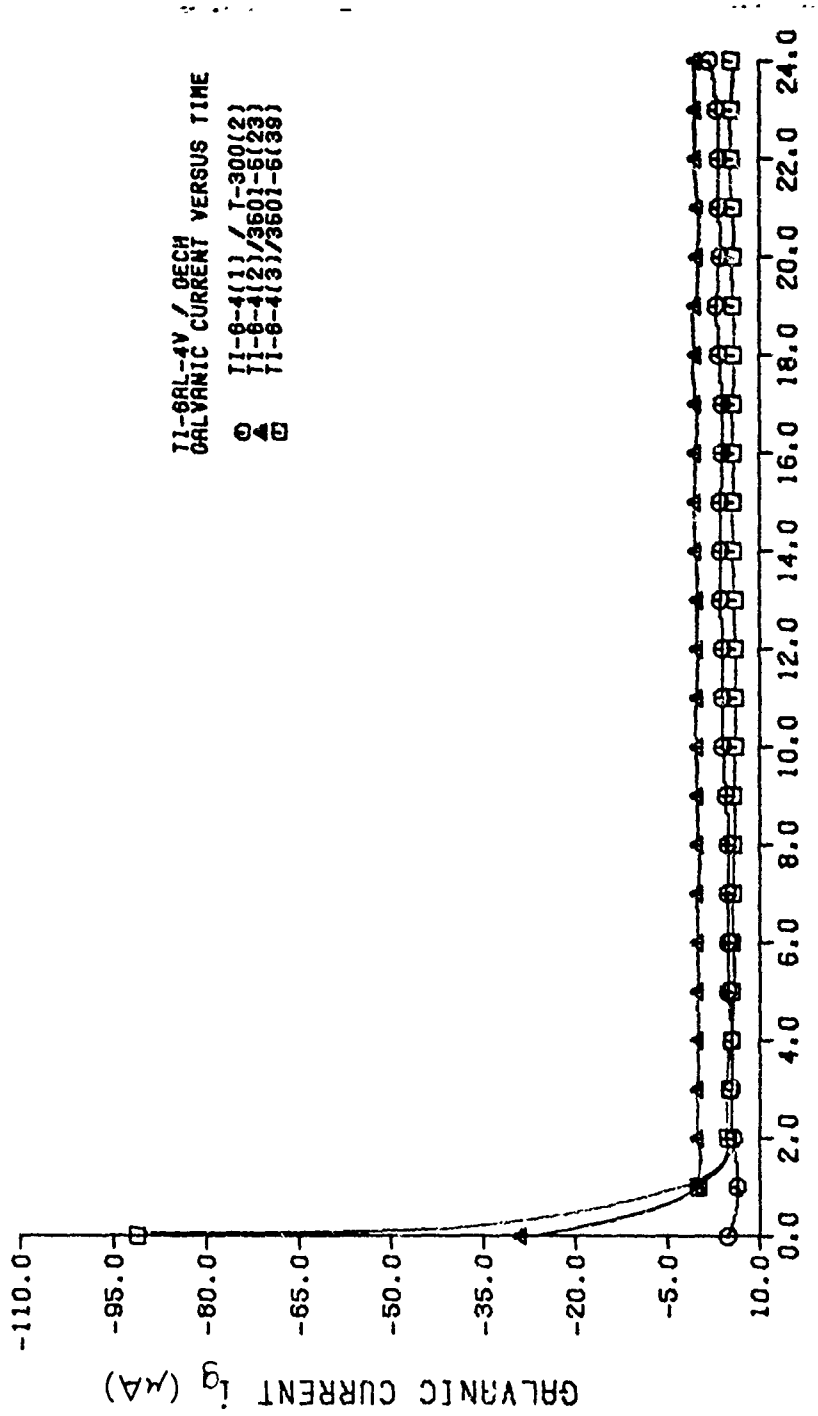

Fig. 39. Galvanic Current vs Time for Ti-6Al-4V/GECM Couples in 3.5% NaCl Solution at Ambient Temperature

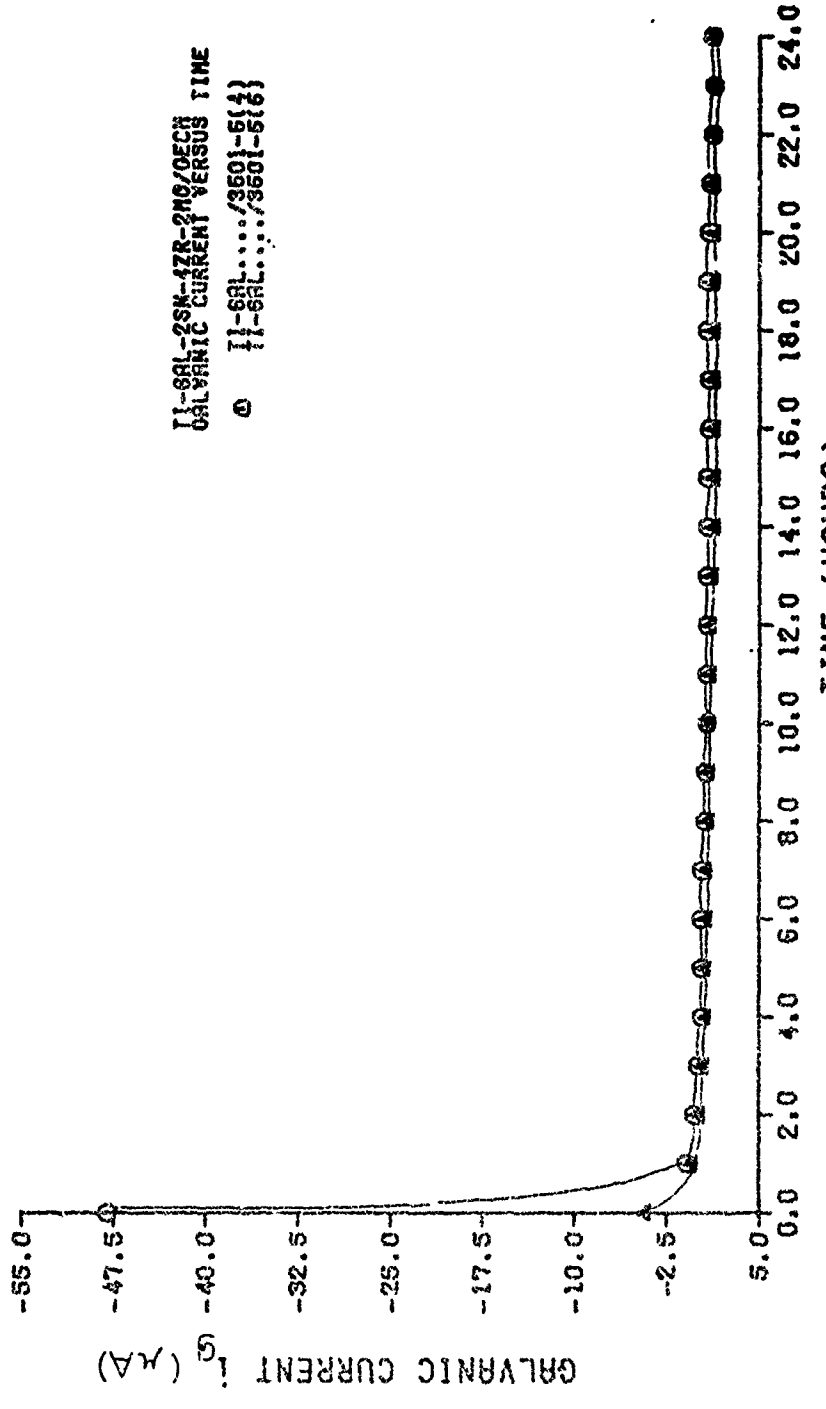

Fig. 40. Galvanic Current vs Time for Ti-6Al-2Sn-4Zr-2Mo / GECM Couples in 3.5% NaCl Solution at Ambient Temperature

Appendix F

Galvanic Current vs Time for
GECM - Be-Cu Couple

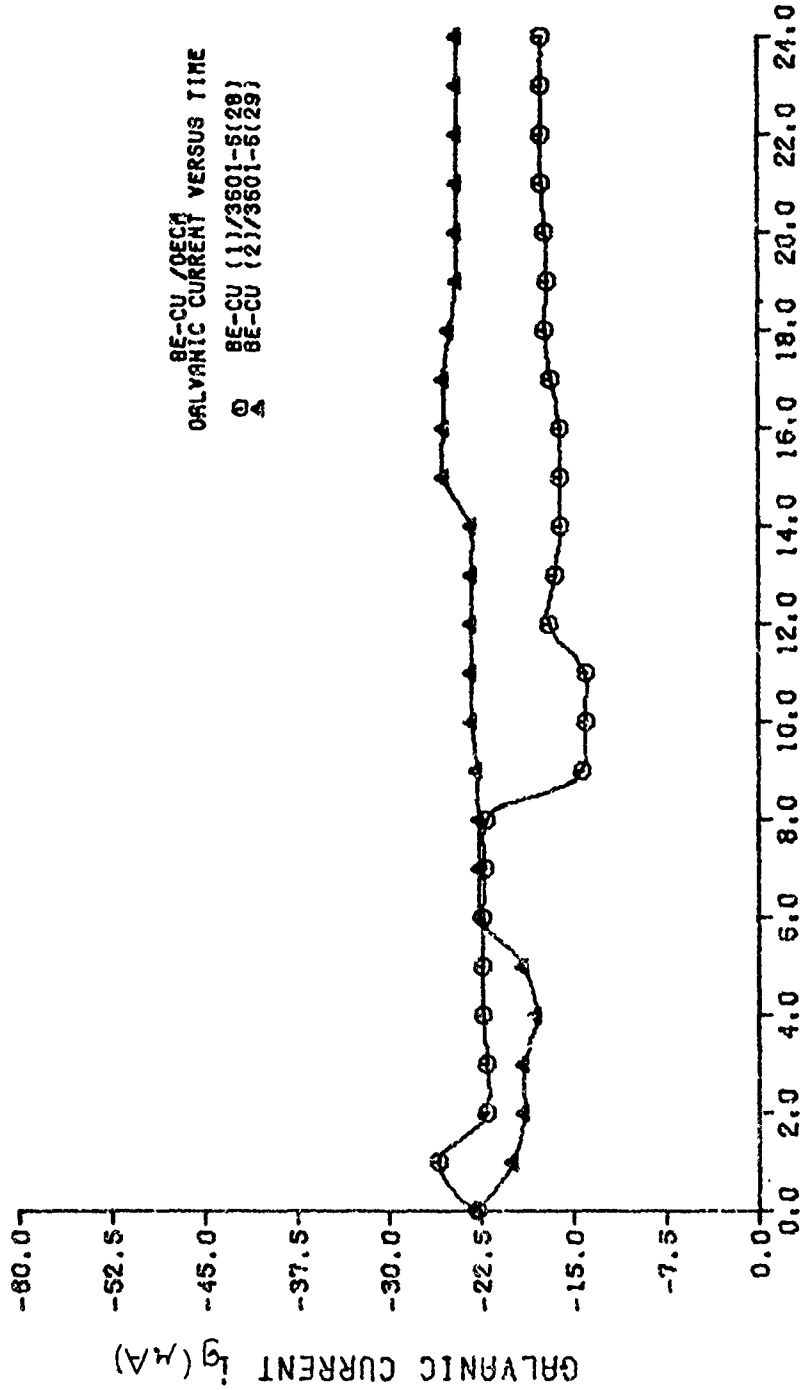

Fig. 41. Galvanic Current vs Time for Be-Cu / GECM Couples in 3.5% NaCl Solution at Ambient Temperature